De novo organelle biogenesis in the cyanobacterium TDX16 released from the green alga *Haematococcus pluvialis*

Qing-lin Dong*, Xiang-ying Xing, Yang Han, Xiao-lin Wei, Shuo, Zhang

Department of Bioengineering, Hebei University of Technology, Tianjin 300130, China

*Correspondence: qldong@hebut.edu.cn

Abstract

It is generally accepted that eukaryotes originate from prokaryotes, which can achieve only by development of organelles in the latter. Such events, however, have not been observed. Here, we report the formation of organelles in the cyanobacterium TDX16 that was released from the senescent/necrotic cell of green alga *Haematococcus pluvialis* (host). Organelle biogenesis was initiated with cytoplasm compartmentalization, followed by partial de-compartmentalization, DNA fragmentation, aggregation and allocation, and re-compartmentalization, as such two compound organelles-the primitive chloroplast (PC) with a minor portion of DNAs and the primitive nucleus (PN) sequestering the major portion of DNAs were formed. Thereafter, the eukaryotic cytoplasm was built up from the matrix extruded from PN; mitochondria were assembled in and segregated from PC, whereby PN and PC matured into nucleus and chloroplast respectively. Most of the mitochondria turned successively into double-membraned vacuoles after matrix degradation, which along with the two sets of nuclear envelops and double-membraned cytoplasmic envelope mediate conventional and unconventional exocytosis and endocytosis. Results of pigment analyses, 16S rRNA and genome sequencing revealed that TDX16 is a phycocyanin-containing cyanobacterium resembling *Chroococcidiopsis thermalis*, which had acquired 9,017,401bp DNAs with 10301 genes form its host. Hence, organelle biogenesis in TDX16 was achieved by hybridizing the acquired eukaryotic DNAs with its own ones and expressing the hybrid genome. The biogenesis of organelles in TDX16 results in its transition into a new eukaryotic alga and thus has profound implications in cell biology, particularly cancer cell biology, and evolutionary biology: (1) the formation and maturation of the small organelle-less nascent cancer cells share striking similarities with TDX16 development and transition, so, it is most likely that cancer cells arise from bacteria; (2) new single-celled eukaryotes can be formed from prokaryotes, whose evolutionary history can not be reconstructed by gene or genome-based phylogenetic analyses.

Key words: Organelle biogenesis; Cyanobacterium; DNA acquisition; Hybridization; Transition

1. Introduction

All cells are structurally categorized into two groups: eukaryotic cells and prokaryotic cells. Eukaryotic cells contain membrane-bounded organelles. So, organelle biogenesis is crucial for cell maintenance and proliferation, which was previously thought to be achieved only by fission of the preexisting one. Nonetheless, recent studies demonstrated that organelles in the secretory pathway can be formed de novo, including Golgi apparatus (Lippincott-Schwartz and Zaal 2000; Bevis et al., 2002), peroxisomes (South and Gould 1999; Kim et al., 2006; van der Zand et al., 2012; Sugiura et al., 2017); lysosomes (Saftig and Klumperman 2009) and vacuoles (Hoh et al., 1995; Marty 1999; Viotti et al., 2013). These results imply that, provided with the information encoded in the genetic material and the machinery needed to interpret this, the cell can produce the organelle with no information in the form of a template or copy of the organelle (Lowe and Barr 2007).

In sharp contrast to eukaryotic cells, prokaryotic cells have no organelle. It is generally accepted that eukaryotic cells originate from prokaryotic cells, which means that the defining organelle-nuclei can be developed in the latter. Nevertheless, such events have not been witnessed. The reasons for this may be that organelle biogenesis in prokaryotic cells occur quickly under certain conditions, which result in the sudden transition of prokaryotic cells into eukaryotic cells and thus are hard to capture.

In our previous study we found unexpectedly that the senescent/necrotic cells of unicellular green alga *Haematococcus pluvialis* burst and liberated countless small blue cyanobacterial cells (TDX16) in the adverse conditions of high temperature and low irradiance (Dong et al., 2011). TDX16 is light-sensitive, which is relatively stable in the dim light, but turns readily and quickly into small green alga-like cell as light intensity elevated. TDX16's transition was puzzling, which prompted us to investigate if, how and why organelles were formed in its prokaryotic cell.

2. Results

2.1 Unusual structure and variable nature of TDX16

Under low light condition, TDX16 cells were always surrounded by thick sheaths (extracellular matrix) and further enclosed within the sporangia (Fig.1-2), showing some similarities to the endospores (baeocytes) of *Chroococcidiopsis* (Caiola et al., 1993; Billi et al., 2000). Most unusually, cells in the same or different sporangia remained at different developmental states with some different inclusions (Fig.1-2). As shown in Fig.1, three different-sized cells (endospores) in a multilayered sporangium were all devoid of thylakoid, but contained one or two

membrane-limited heterogenous globular bodies (HGB), and a varied number of cyanobacterial inclusions, including carboxysomes (CX) (Yeates et al., 2008), polyphosphate bodies (PB) (Allen 1984), osmiophilic granules (lipid globules/bodies, OG) (Lang 1968). HGB contained DNA-like electron-dense granules and filaments and always situated in the nucleoids (NU), where DNA fibers (DF) (Eltsov and Zuber 2006) and ribosomes (RB) (van de Meene et al., 2006) scattered. The important difference among these cells was that some small swirly and rod-shaped electron-transparent vesicles (EV) were being developed in the left large cell. Similarly, in another five-cell-containing sporangium (Fig.2), the bottom cell contained only OG, while many large different-shaped EV were being formed in the three middle cells, and several thylakoid-like structures were built up in the upper cell.

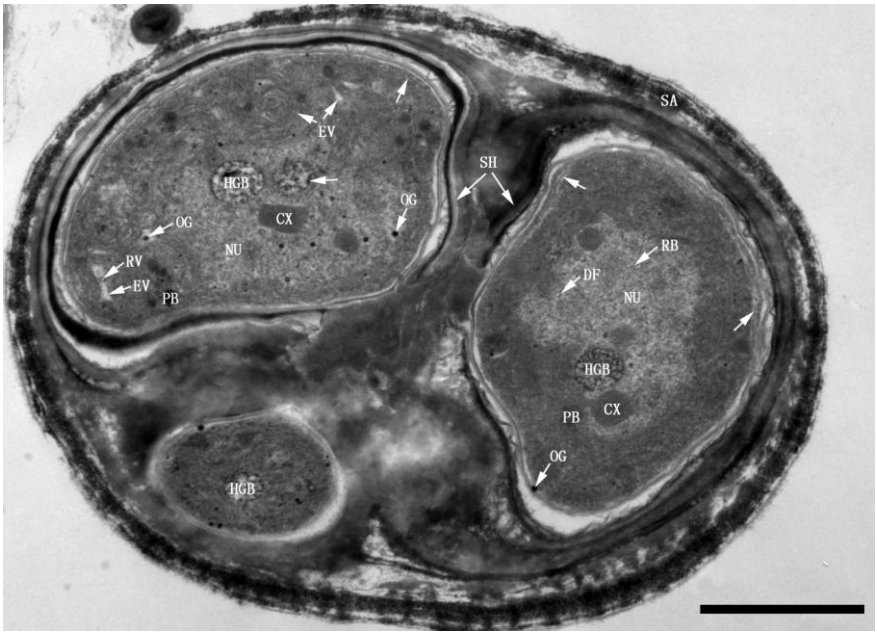

Figure1. Three TDX16 cells within a sporangium (SA). TDX16 cells were enclosed by thick sheaths (SH), containing heterogenous globular bodies (HGB), carboxysomes (CX), ribosomes (RB), DNA fibers (DF) and osmiophilic granules (OG) in the nucleoids (NU) as well as polyphosphate bodies (PB) in the cytoplasm. OG also presented in cytoplasm and some small electron-transparent vesicles (EV) with internal ring-shaped vesicles (RV) or OG were being formed in the upper left cell. Compartmentalization was just initiated in the two large cells (arrow). Scale bar, 1μm.

It was evident that EV developed from OG, because (1) OG presented in the small EV, some of them were, however, not in the section plane and thus invisible; (2) as EV enlarged, OG turned into ring-shaped vesicles (RV) after their dense matrixes degraded into to opaque and finally transparent materials (Fig.1-2). OG contained triacylglycerol and tocopherol (Peramuna and Summers 2014), while its exact composition and structure was as yet unknown. There was a general consensus that OG in cyanobacterial cell was comparable to plastoglobuli (PG) in algal and plant chloroplasts (Lang, 1968; Brehelin et al., 2007), which contained lipids, enzymes,

proteins e.g., IM30/ Vipp1 protein (vesicle-inducing protein in plastids 1) and carotenoids, and structurally consisted of a monolayer lipid membrane (half-unit membrane) and a neutral lipid core (Austin et al., 2006; Ytterberg et al., 2006; Vidi etal., 2006; Lichtenthaler 2013; Davidi et al., 2015). Nevertheless, the formation of RV in EV indicated that OG had two monolayer lipid

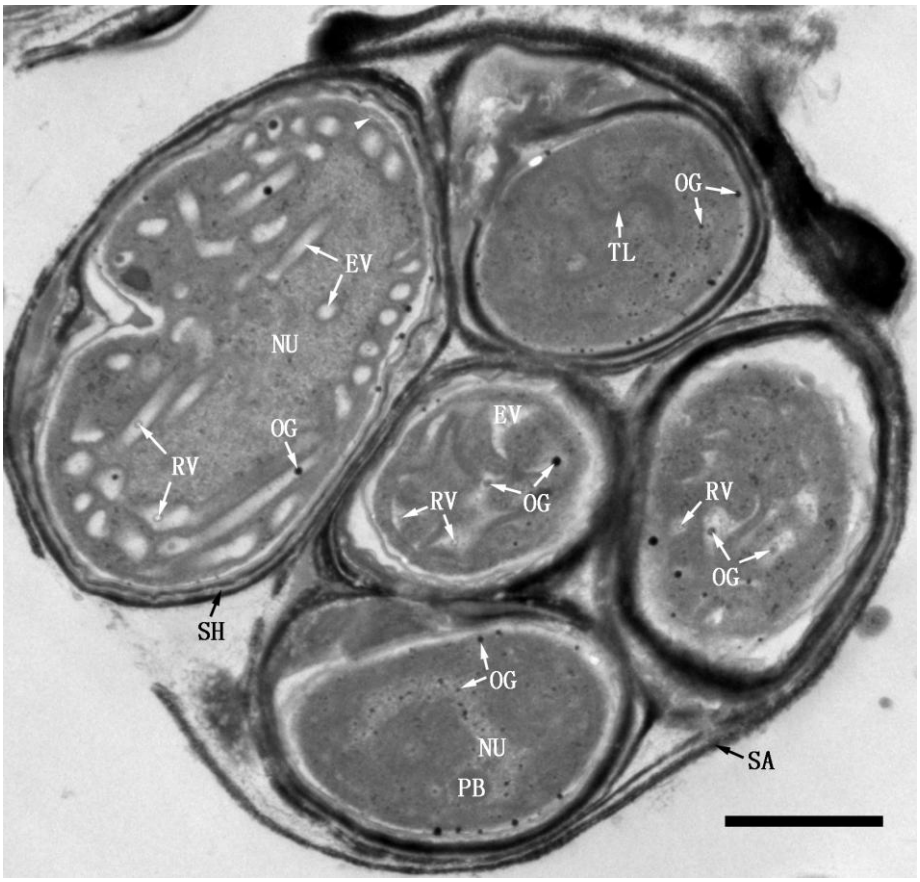

Figure 2. Five TDX16 cells within a SA. The bottom cell was devoid of EV, while a great number of EV were being developed in the three middle cells, and several thylakoid-like structures (TL) were built up in the upper cell. Compartmentalization commenced in the large cell (arrowhead). Scale bar, 1μm.

membranes, which most likely encased a hydrophilic "protein core", while the intermembrane space was filled with neutral lipids. So, as the intermembrane space dilated owing to the synthesis of low-density lipids or the like, the outer monolayer membrane bulged and gave rise to an EV; while the interior monolayer membrane and the protein core remained as a monolayer membrane-bounded OG, which subsequently transformed into a RV after the protein core was metabolized or transformed (Fig.1-2).

The above results demonstrated that unlike the genuine thylakoid-less cyanobacterium *Gloeobacter violaceus* (Rippka et al., 1974), TDX16 was hypersensitive to light and highly variable in nature, whose anomalous change could not be inhibited completely even in the dim light. Therefore, it was not surprising that when grew in high light regime, TDX16 changed fundamentally in cell structure and pigmentation, which were described in the following sections.

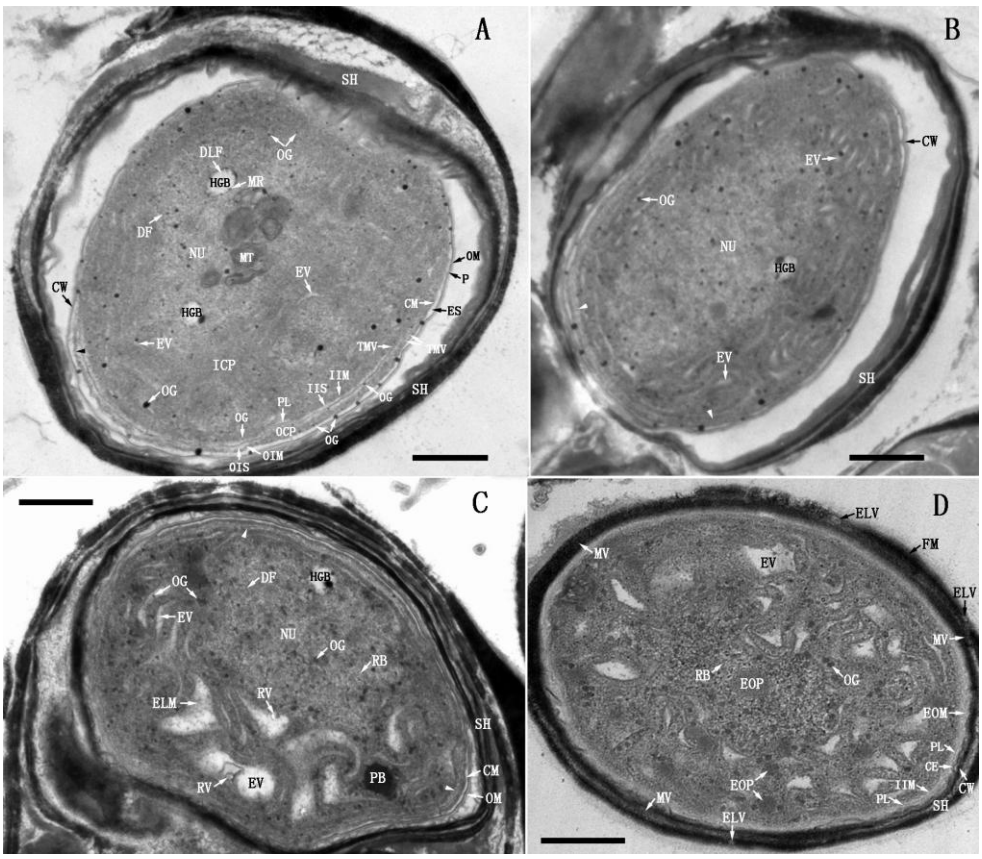

Figure 3. Compartmentalization, formation of EV and cytoplasmic envelope. (**A**) TDX16's cell wall (CW) comprised an outer membrane (OM) and a peptidoglycan layer (P), which was separated from the cytoplasmic membrane (CM) by an extracytoplasmic space (ES). Inside the cytoplasm, an inner intracytoplasmic membrane (IIM), an outer intracytoplasmic membrane (OIM) and an intervening peptidoglycan-like layer (PL) were being synthesized by fusion of the small thick margin vesicles (TMV) blistered form the inner leaflet of the cytoplasmic membrane. Whereby, the cytoplasm was partitioned into three compartments: the inner cytoplasm (ICP); the outer cytoplasm (OCP), and the sandwiched intracytoplasmic space (IS) that was further separated by PL into an outer intracytoplasmic space (OIS) and an inner intracytoplasmic space (IIS). OCP began to reduce in localized region near the start point (arrowhead), such that OIM moved to CM. OG budded from the inner leaflet of CM, IIM and OIM, and migrated into ICP, where many small EV were being formed and stacks of membranous elements (MT) emerged; while HGB became nearly empty leaving only DNA-like fibrils (DLF) and electron-dense margin residues (MR). Interestingly, OG shed from the outer leaflet of CM into ES, connecting CM and CW. (**B**) IS became narrow (arrow), while more and more small EV were being developed from OG. (**C**) EV dilated into swirling ones spiraling around NU, but IS still remained narrow. (**D**) When EV was formed in NU, several electron-opaque particles (EOP) emerged, while IS became widened filling with electron-opaque materials (EOM). Importantly, OCP disappeared such that OIM and CM were positioned together, and became a double-membraned cytoplasmic envelope (CE). Some electron-dense materials were synthesized on CE and transferred to CW for assembling SH, which was made up of flocculent fibrillary materials (FM), microvesicles (MV) and electron-translucent vesicles (ELV). Scale bar, 0.5 μm.

2.2 Compartmentalization and biogenesis of primary thylakoids

2.2.1 Compartmentalization by synthesizing intracytoplasmic membranes

Under high light intensity, TDX16 with surrounded sheath escaped from the ruptured sporangium and changed rapidly in structures and inclusions (Fig.3A). PB and CX disappeared, HGB became nearly empty leaving only few DNA-like fibrils and electron-dense margin residues; while a startling number of OG and stacks of membranous elements emerged, and many small EV were being developed (Fig.3A). The most striking change was, however, the compartmentalization of cytoplasm that was enclosed by the cytoplasmic membrane (CM) (Fig.3A). TDX16's cell wall, like those of other cyanobacteria (Hoiczyk and Hansel 2000; Liberton et al., 2006), comprised an outer membrane (OM) and an electron-dense peptidoglycan layer (P), which was separated from CM by an electron-transparent extracytoplasmic (periplasmic) space (ES) (Fig.3A). Inside the cytoplasm, two intracytoplasmic membranes and an intervening peptidoglycan-like layer (PL) were being synthesized, which initiated from a start point and extended parallel to CM (Fig.3A). As a result, the cytoplasm was partitioned into three compartments: (1) the inner cytoplasm (ICP) delimited by the inner intracytoplasmic membrane (IIM), (2) the outer cytoplasm (OCP) of variable thickness bounded by the outer intracytoplasmic membrane (OIM) and CM, and (3) a sandwiched intracytoplasmic space (IS) that was further separated by PL into an outer intracytoplasmic space (OIS) and an inner intracytoplasmic space (IIS) (Fig.3A). It was important that OCP began to reduce or degrade in localized regions near the start point, such that OIM got closed to but not connected with CM (Fig.3A). Compartmentalization also commenced in some cells growing in the low light just as the formation of EV (Fig.1-2). In all these cases, there was no continuity between the intracytoplasmic membranes and CM, and thus the formers were not developed by invagination of the latter. Instead, OIM, IIM and PL were synthesized synchronously by fusion of the small thick margin vesicles (TMV) blistered form the inner leaflet of CM (Fig.3A) in two probable ways: (1) if TMV were delimited by a half-unit membrane, they first released their contents for synthesizing the septal PL and then fused alternately on its two sides; (2) if TMV were limited by a unit membrane, as they fused one another, the septal PL was synthesized within the coalesced vesicles, a scenario somewhat similar to the formation of cell plate during cytokinesis (Samuels et al., 1995).

2.2.2 Production of OG

Concurrent with compartmentalization, plentiful OG of various sizes blistered from the inner and outer leaflets CM (Fig.3A), such a scenario was also observed in the cells growing under low light condition (Fig.1-2). More importantly, some small OG also budded from the inner leaflet of OIM and outer leaflet of IIM (Fig. 3A). These results suggested that the newly formed OIM and IIM were comparable or equivalent to the multifunctional CM, on which both photosynthesis and respiration performed just like the case of the cytoplasmic membrane of *Gloeobacter violaceus*

(Rippka et al., 1974; Rexroth et al., 2001). OG was formed by protrusion of the bilayer of CM, OIM and IIM as they were enclosed by two half-unit membranes (Fig.1-2) and apparently played different roles. OG blistered from the inner leaflet of CM, OIM and IIM migrated into ICP for development of EV (Fig.3A); while those shed from the outer leaflet of CM contacted CW, and thus severed as transport conduits or trafficking vehicles channeling or transferring lipids and carotenoids from CM to the CW (Fig.3A), because these compounds were the constituents of OM (Hoiczyk and Hansel 2000).

2.2.3 Formation of EV and double-membraned cytoplasmic envelope

As OIM, IIM and PL extended (Fig.3B) and ultimately closed up (Fig.3C), the small EV elongated (Fig.3B) and dilated asymmetrically into swirling ones spiraling around NU, and OG began to merge into large ones (Fig.3C). Thereafter HGB disappeared, while new EV were developed within NU and several electron-opaque particles (EOP) were formed (Fig. 3D). In parallel with these changes, the narrow IS (Fig. 3BC) became widened filling with electron-opaque materials (EOM) (Fig. 3D), while OCP disappeared, such that OIM and CM combined into a double-membraned cytoplasmic envelope (CE), which abutted CW owing to the narrowing of ES (Fig.3D). During this process a mass of electron-dense materials were synthesized on CE and transferred to CW for assembling SH, and thus made these structures indistinct (Fig.3D). SH was loosely compacted, made up of flocculent fibrillary materials (FM), microvesicles (MV) and electron-translucent vesicles (ELV) (Fig.3D).

2.2.4 Development of EV into primary thylakoids

The intraluminal RV swelled up into a dilated-ring-shaped vesicle (DRV), whose membrane ultimately met and combined with EV membrane, giving rise to a unit-membrane-bounded combined vesicle (CV); and then CV coalesced into long ones or flattened out into short slender sacs, termed primary thylakoids (PT) (Fig.4A). In this way, EV developed progressively into short PT with opaque matrix, distributing randomly in ICP (Fig.4B). The short PT further extended or merged end-to-end into long PT; while the long coalesced CV flattened out into PT by localized-constriction. And concurrently several cyanophycin granules (CG) (Simon 1971) and EOP were formed (Fig. 4C). Finally, the long PT were adjusted to be parallel-arranged, on which the extrinsic phycobilisomes (PCB) (Gantt and Conti 1969) were assembled (Fig.4D).

2.3 De-compartmentalization, DNA translocation, re-compartmentalization and biogenesis of secondary thylakoids

2.3.1 De-compartmentalization and decondensation of ICP and DNA translocation

The newly formed PT promoted TDX16's photosynthetic capacity, but were disassembled soon afterwards. As shown in Fig.5A, PT disassembly initiated with the condensation of luminal matrix, such that PT membrane pair was in closely apposition, seeming to be a single membrane with rough margin. In the meantime, ICP decondensed (solubilized) and became translucent, in which

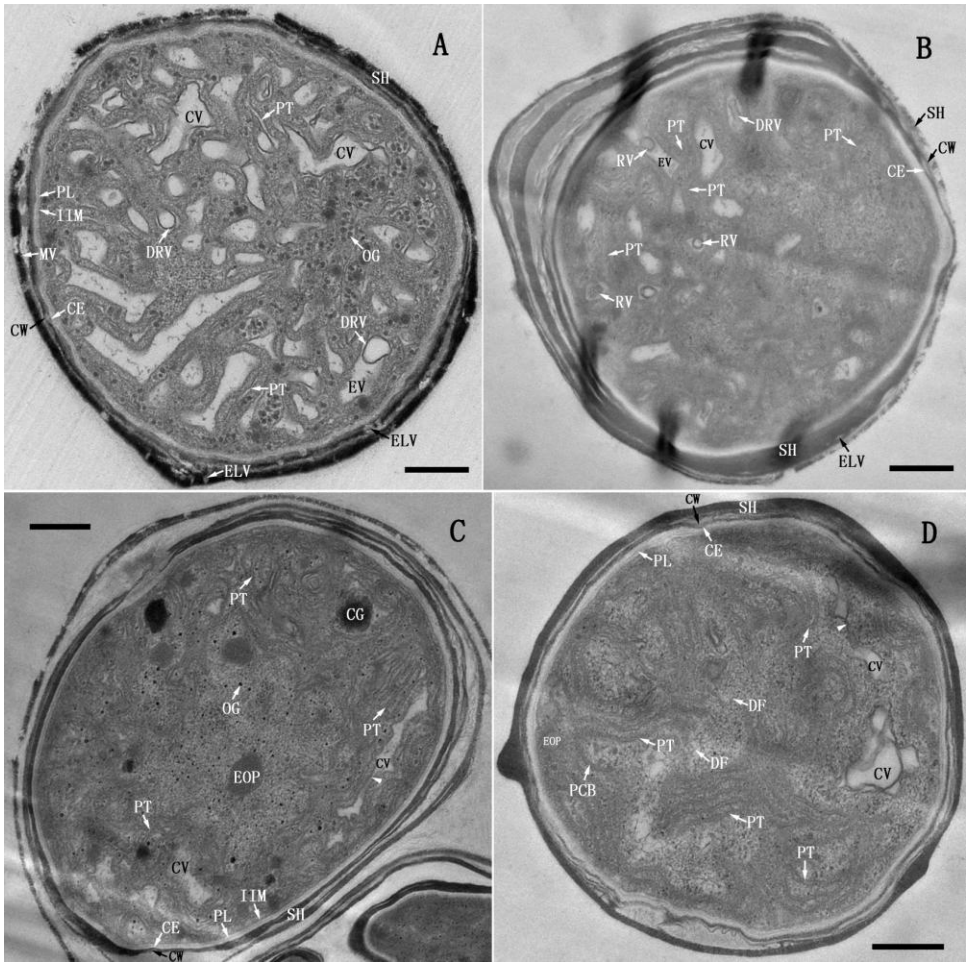

Figure 4. Development of EV into primary thylakoid. (**A**) RV swelled into dilated-ring-shaped vesicle (DRV), whose membrane met ultimately with EV membrane, and thus gave rise to a unit-membrane-bounded combined vesicle (CV). Subsequently, CV coalesced into longer ones or flattened out into slender short primary thylakoids (PT). (**B**) The newly formed short PT distributed randomly in ICP, whose matrix turned opaque. Occasionally a cluster of small RV presented in a EV. (**C**) The short PT extended or merged end-to-end into long PT; while the long coalesced CV flattened out into PT by localized-constriction (arrowhead).Meanwhile, several cyanophycin granules (CG) were formed. (**D**) PT became parallel-arranged with wide spacing, on which the extrinsic phycobilisomes (PCB) were assembled. Scale bar, 0.5 μm.

short DF dispersed, some less electron-dense materials (LDM), less electron-dense bodies (LDB) and CG were formed (Fig.5A); IIM disassembled into tiny vesicles (TV), such that ICP de-compartmentalized, LDM diffused outward, blurring the compacted PL, CE and CW (Fig. 5A). Subsequently, the solubilized ICP was separated into two portions by LDM: in the lower portion, PT broke up into double-layered membrane fragments (DMF, two unit membranes) and in parallel

DF aggregated; while in the upper portion, DMF began to curl and merge laterally into double-membraned vesicles (DMV) (Fig.5B). When all DMF disappeared, a crowd of DMV was formed and numerous DF aggregated (Fig.5C). Thereafter, DMV moved outward quickly and attached to PL that was cover by electron-dense materials, while the intermingled DF scattered outward slowly resulting in an “empty” inner space (EIS), at the border of which the recruited TV began to fuse into double-layered membrane segments (DMS) (Fig. 5D).

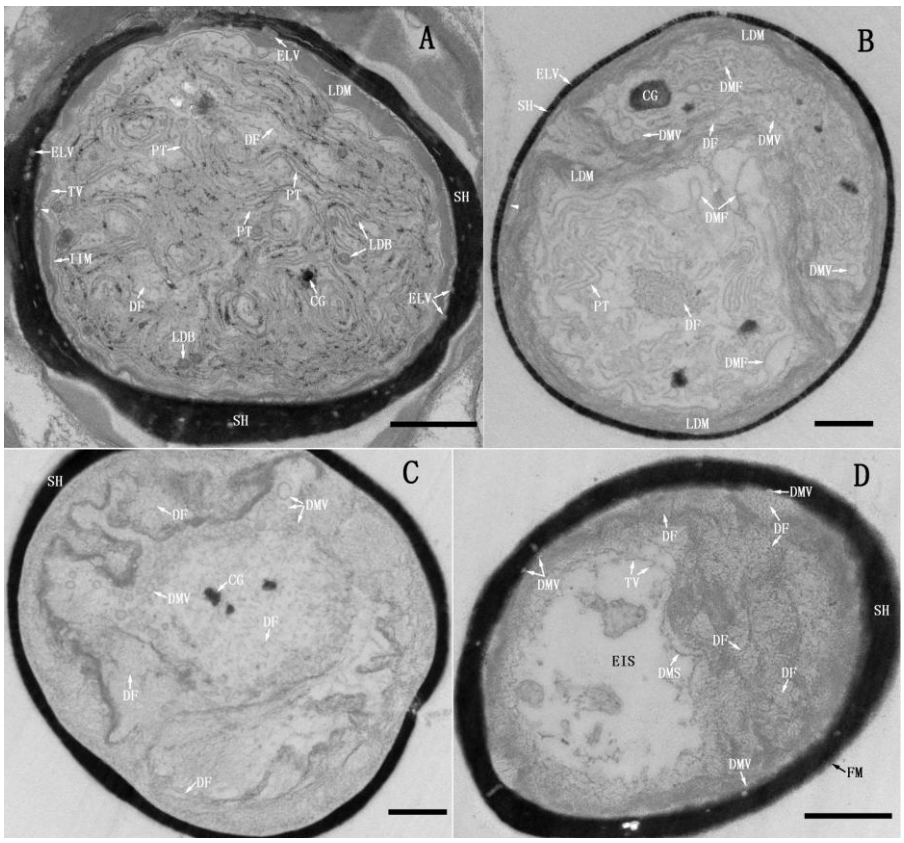

Figure 5. Decondensation of ICP, disassembly of IIM and PT, and translocation of DNA. (**A**) IIM broke down and rounded up into tiny vesicles (TV); PT matrix condensed and thus the membrane pair were in close apposition with concurrent disassembly of PCB; ICP decondensed and became translucent, in which short DF dispersed, and some less electron-dense materials (LDM) and less electron-dense bodies (LDB) were formed. LDM diffused outward and blurred the compacted PL, CE and CW (arrowhead). (**B**) PT broken up into double-layered membrane fragments (DMF), which began to merge laterally into double-membraned vesicles (DMV); while DF aggregated into a cluster. (**C**) All PT transformed into DMV, dispersing along with the aggregated DNA fibers in the decondensed ICP. (**D**) DMV moved outward and attached to PL that was cover by electron-dense materials, while the intermingled DF scattered outward slowly resulting in an “empty” inner space (EIS), at the border of which the recruited TV began to fuse and elongate into double-layered membrane segments (DMS). Scale bar, 0.5 μm.

2.3.2 Re-compartmentalization, DNA reallocation and formation of secondary thylakoids

As DMS coalesced and extended into a double-membraned intracytoplasmic envelope (ICE), the coalesced ICP and IIS was re-compartmentalized into a new inner cytoplasm (NIC) and a new inner intracytoplasmic space (NIS) (Fig.6A). NIC was enclosed by ICE; while NIS represented the

space between ICE and PL. Most DF was allocated into NIS, which decondensed into cloudlike materials or aggregated into thick threads; by contrast only few sporadic DF and electron-dense particles (EP) were portioned into NIC (Fig.6A). ICE was not sealed, on the outer leaflet of which,

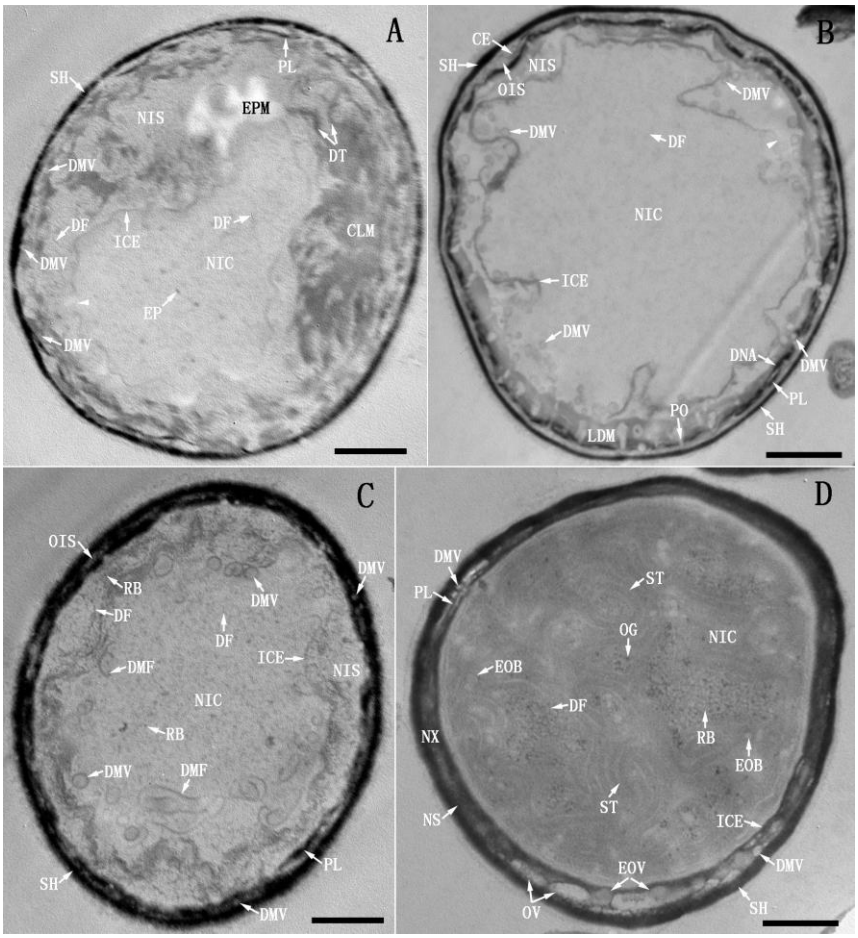

Figure 6. Re-compartmentalization, reallocation of DNA and formation of secondary thylakoids. (**A**) As DMS extended into a double-membraned intracytoplasmic envelope (ICE), a new inner cytoplasm (NIC) and a new inner intracytoplasmic space (NIS) were re-compartmentalized. Most of the DNA fibers were relocated in NIS, which decondensed into cloudlike materials (CLM) or aggregated into DNA threads (DT). By contrast only few DF and electron-dense particles (EP) were partitioned into NIC. ICE was not sealed, so substances could be exchanged through its opening (arrowhead). Interestingly, some electron-transparent materials (EPM) were synthesized on the outer leaflet of ICE. (**B**) Accompanying the expansion of ICE, DMV in NIS moved into NIC via ICE opening (arrowhead), or passed through PL pores (PO) into OIS. (**C**) After ICE sealed, DNA in NIS recondensed into a mass of DF with concomitant formation of countless RB. Meanwhile, an increased number of DF emerged and some RB were formed in NIC; DMV began to open up and re-transformed into DMF and elongated. (**D**) DMF in NIC extended into PCB-less secondary thylakoids (ST) with concomitant formation of OG and electron-opaque bodies (EOB) as well as enrichment of DF and RB. Outside of NIC, the major portion of PL was dismantled, such that NIS and OIS coalesced into a new intracytoplasmic space (NS), whose confluent content became the new intracytoplasmic matrix (NX). Aside from DMV, electron-translucent oblong vesicles (OV) and electron-opaque vesicles (EOV) emerged in NS. Scale bar, 0.5 μm.

some electron-transparent materials were synthesized (Fig.6A), similar in appearance to the

bacterial lipid (Alvarez et al., 1996). Accompanying ICE expansion, DF in the narrowing NIS decondensed and attached to the thickened PL (Fig.6B); while DMV that were covered by LDM detached from PL, moving inward via ICE opening into NIC or outward through PL pores into OIS (Fig.6B). Therefore, the fenestrated PL served not only as a mechanical and osmotic barrier, but also a platform for anchoring DNA and DMV. When ICE was sealed, DNA in NIS recondensed into thick DF resembling chromatin fibers (Woodcock et al., 1984) with concomitant formation of countless RB (Fig. 6C). Meanwhile, in NIC an increased number of DF and a myriad of RB were also formed; DMV dilated, opened up and retransformed into DMF (Fig. 6C). Thereafter, DMF extended randomly into spiral thylakoids, which was devoid of PCB and morphologically different from PT, termed secondary thylakoids (ST) (Fig.6D). Concomitant with the appearance of ST was the formation of OG and EOB as well as enrichment of DF and RB (Fig.6D). The structures outside of NIC were fuzzy owing to the diffusion of electron-dense materials: the major portion of PL dismantled, such that NIS and OIS coalesced into a new intracytoplasmic space (NS), whose content became the new intracytoplasmic matrix (NX). Aside from DMV, several large electron-translucent oblong vesicles (OV) and electron-opaque vesicles (EOV) emerged in NS (Fig.6D).

2.4 Biogenesis of primitive chloroplast, eukaryotic cell wall and primitive nucleus

2.4.1 Formation of primitive chloroplast and eukaryotic cell wall

Immediately after the emergence of transitional ST, drastic changes occurred in different compartments. As shown in Fig.7A, NIC became polarized, in which ST underwent disassembly, leaving some remnants in the lower region; while parallel arrays of discrete slender sacs with transparent matrix were being developed in the upper region (Fig.7A). These parallel-arranged slender sacs were morphologically similar to algal and plant thylakoids, termed the primitive eukaryotic thylakoids (PMT). Beneath PMT, a nascent pyrenoid (PD) with an incomplete starch plate (SP) and two starch granules (SG) were formed (Fig.7A), both of which were the characteristic bodies of green algal chloroplasts (Gibbs, 1962). So, NIC developed into a primitive chloroplast (PC) delimited by ICE. That was to say, ICE became the chloroplast envelope (CHE). PMT were developed from PG produced during disassembly of ST (Fig.7A), in a way similar but not identical to the biogenesis of PT from OG (Fig.4). The absence of mitochondrion implied that respiration still performed on PMT. Thus, PC was a compound organelle sharing the functions of chloroplast and mitochondrion.

NS became widened and clear: NX condensed, containing RB and chromatin fibers (CF) (Hay and Revel, 1963; Woodcock et al., 1984); PL and DMV disappeared, while many small

dotted vesicles (DV) blistered from CHE and lined up along CE, some of which began to fuse and flattened into membrane segments (MS) (Fig.7A). Such a scenario of membrane synthesis was

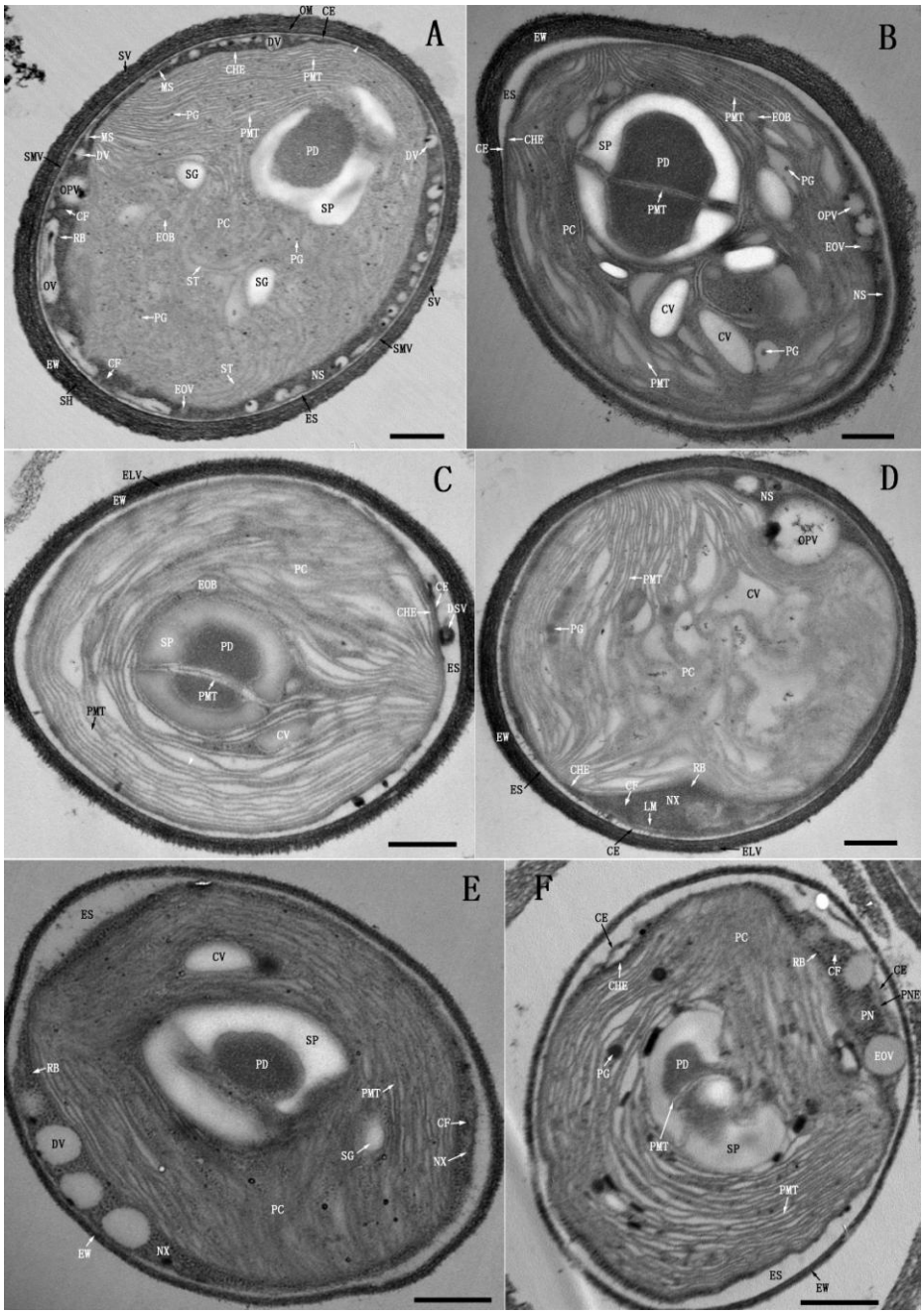

Figure7. Biogenesis of primitive chloroplast, eukaryotic cell wall and primitive nucleus. (**A**) ST was disassembled leaving some remnants in the lower region of the polarized NIC, while parallel arrays of primitive eukaryotic thylakoids (PMT) were being developed from the plastoglobuli (PG) in upper region of NIC with concomitant formation of a nascent pyrenoid (PD) surrounding by an incomplete starch plate (SP), and two starch granules (SG). So, NIC developed into the primitive chloroplast (PC), and ICE became the chloroplast envelope (CHE). Inside NS, thick chromatin fibers (CF) and large RB were formed; PL and DMV disappeared; while many small dotted vesicles (DV) and opaque-periphery vesicle (OPV) emerged. Some DV began to fuse and flattened into membrane segments (MS). Outside of NS, some smaller vesicles (SMV) shed from the outer leaflet of CE into ES; while the peptidoglycan layer (P) of CW turned into an electron-dense layer (EL) (arrowhead), and a stratified

SH embedded with small vesicles (SV) was formed external to OM, hence the compacted CW and SH became the eukaryotic cell wall (EW). (**B**) PMT with wide luminal space were formed continuously by elongation of CV; PD got matured with a complete SP, bisecting by two pairs of PMT. The expanded PC occupied most of NS in longitudinally sectioned plane. (**C**) PC filling with PMT occupied whole NS, such that NS disappeared in longitudinally sectioned plane, CHE adhered to CE, from which a dense vesicle (DSV) shed off into the widened ES. (**D**) A vertical section of cell. The anterior PC portion occupied the surrounding NS, so EX was pushed to the shrinking NS around the posterior portion of PC, at the border of which MS fused into a limiting membrane (LM). (**E**) An oblique section through the posterior half of cell, in which most of the NX aggregated at one side of PC. (**F**) A tangential section through the posterior end of cell. All NX converged at one side of PC, which was encased by LM and thus turned into the primitive nucleus (PN) containing CF, RB and EOV; while LM became the primitive nuclear envelope (PNE). NS vanished and in turn CE shrank and wrapped PC and PN. Scale bar, 0.5 μm.

akin to the assembly of nuclear envelope in vivo and in vitro (Forbes et al., 1983; Lohka and Masui 1984). Furthermore, a large coated-vesicle-like opaque-periphery vesicle (OPV) was being assembled at CHE, which appeared to bridge CHE and CE for transferring substances.

The fluffy SH (Fig.6D) was organized into a multilayered one, which adhered to OM and made the latter hard to discern (Fig.7A). Such that the new stratified SH and CW seemed to be a continuum (entity), similar in appearance to the cell wall of eukaryotic cell, referred to as the eukaryotic cell wall (EW). The formation of new SH implied that CE and OM were remodeled, while the peptidoglycan layer (P) underlying OM turned into an electron-dense layer (EL).

2.4.2 Encapsulation of the concentrated NX into primitive nucleus

As PG developed progressively into CV and then flattened into PMT with wide luminal space in the lower PC region, PD got matured, surrounded with a complete SP and bisected by two pairs of PMT. Hence, PC expanded substantially, occupying most NS (Fig.7B). Subsequently, PMT coalesced and extended around PD (Fig.7C). The membranes of adjacent PMT were connected, giving the appearance to be a single membrane. So, PC expanded further and occupied whole NS in the longitudinally sectioned planes; CHE adhered to CE, from the latter of which a dense vesicle (DSV) shed off into the widened ES (Fig.7C).Vertical profile (Fig.7D) showed that the anterior portion of NS disappeared owing to PC expansion, such that NX in the shrunken NS was concentrated by squeezing out liquid into ES, at the border of which MS coalesced into a limiting membrane (LM) (Fig.7D). As PC expansion continued, the stepwise-concentrated NX moved to (Fig. 7E) and finally converged at one side of PC, which was ensheathed by LM and turned into the primitive nucleus (PN) (Fig. 7F). Consequently, LM became PN envelope (PNE), NS vanished, and in turn CE shrank and wrapped PC and PN (Fig. 7F).

2.5 Formation of eukaryotic cytoplasm and biogenesis of mitochondrion

2.5.1 Concurrent formation of eukaryotic cytoplasm and biogenesis of mitochondria

As shown in Fig.8A, a vesicle-containing body (VB), apparently derived from the invaginated PC, was being engulfed by PN with concomitant formation of a thin layer of electron-dense materials.

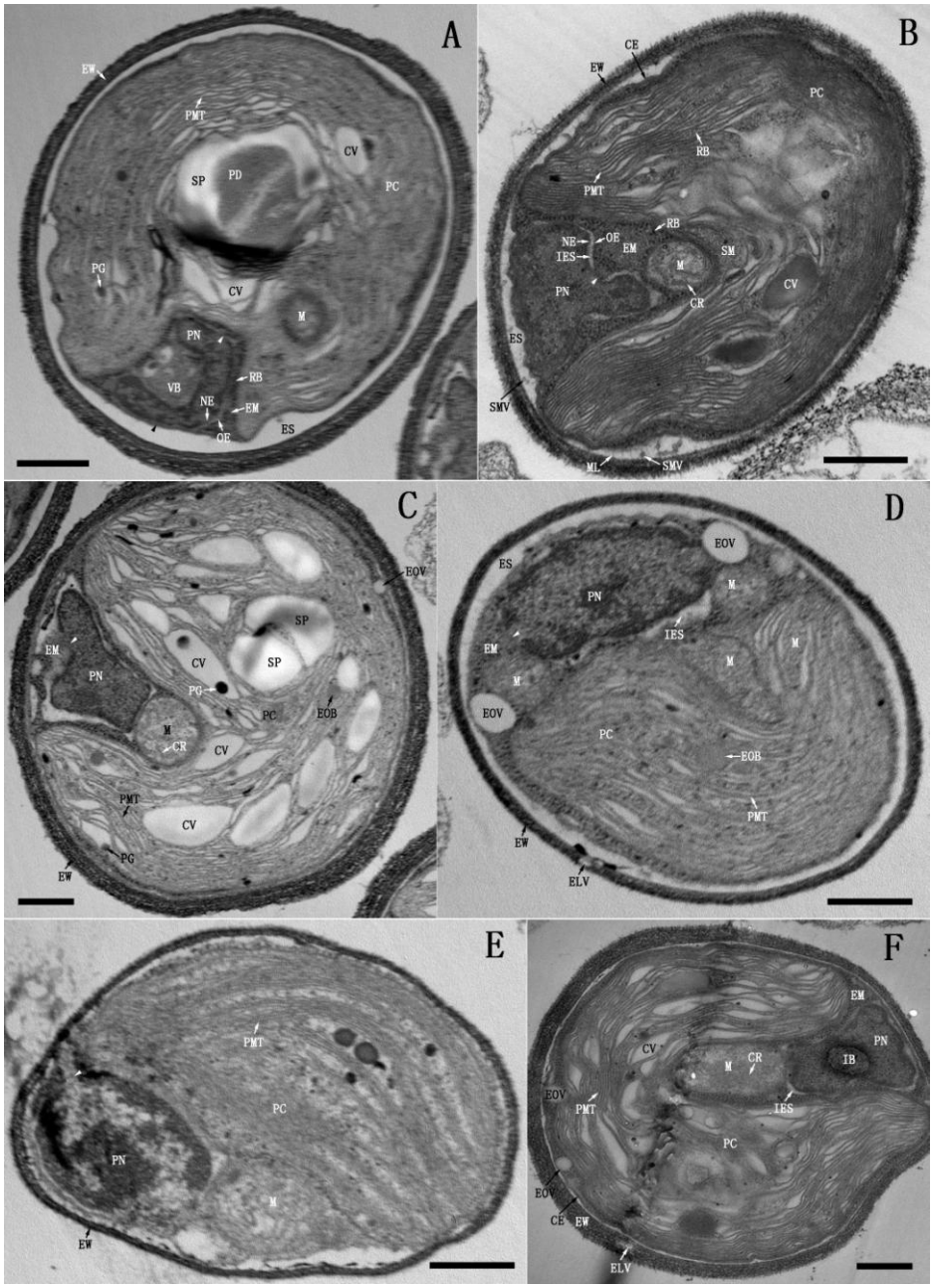

Figure 8. Concurrent formation of eukaryotic cytoplasm and biogenesis of mitochondria. (**A**) PN was engulfing a vesicle-containing body (VB) with concomitant extrusion of nuclear matrix, i.e. the eukaryotic cytoplasm (EM). PNE comprised a nuclear envelope (NE) and an outer nuclear envelope (OE), which was contiguous with CE at the outer side (black arrowhead), but separated in PC cavity. EM was extruded from PN at the site where NE and OE fused (white arrowhead), and concurrently a mitochondrion (M) was assembled in PC. (**B**) PC with enriched stroma (SM) further invaginated, in the apical dome of its cavity, a mitochondrion with characteristic cristae (CR) emerged. OE and NE of the enlarged PN were separated by an inter envelope space (IES), but came into contact a one site and fused into a large opening (arrowhead), from which the nuclear matrix (i.e. EM) was expelled. In the meantime, a number of SMV and microfibrils (ML) budded and emanated from CE into ES. (**C**) PN expelled EM from the fused opening of NE and OE (arrowhead) in the presence of a newly

formed spherical mitochondrion. (**D**) A large PN extruded EM (arrowhead) in the presence of two mitochondria, while two spindle-shaped mitochondria were being assembled within PC. (**E**) PN expelled EM (arrowhead) coincident with the appearance of a spindle-shaped mitochondrion. (**F**) A large PN contained a membrane-delimited intranuclear body (IB). Scale bar, 0.5 μm.

PNE was contiguous with CE at the outer side, but separated into two sets of double membraned envelopes inside PC cavity, the inner and outer sets of which were referred to as nuclear envelope (NE) and outer nuclear envelope (OE) respectively. This result confirmed that PNE was consisted of four unit membranes. The thin layer of electron-dense materials was extruded from PN at the site where NE and OE fused, which contained RB and thus was the nascent eukaryotic cytoplasm (EM). Concurrent with the formation of EM, a small mitochondrion (M) was being assembled in PC. After 'digestion' of VB, PN and EM both increased in sizes; and an oval mitochondrion with characteristic cristae (CR) emerged in the apical dome of the enlarged PC cavity (Fig.8B). NE and OE were separated by an interenvelope space (IES), but merged at one site resulting in a wide opening, from which nuclear matrix (i.e. EM) was extruded. RB in EM were larger than those within the PC stroma (SM), most of which were attached to the organelles (Fig.8B). During this process, a number of SMV and microfibrils (ML) budded and emanated from CE into ES (Fig.8B). Concurrent nuclear matrix extrusion and mitochondrion formation were observed in different cells (Fig. 8CDE), and two spindle-shaped mitochondria were just being assembled in a PC (Fig. 8D). Occasionally, an intranuclear body (IB) appeared in a PN (Fig.8F), which seemed to be developed during engulfment and digestion of VB, and play a role in selective extrusion of nuclear matrix.

2.5.2 Continuous biogenesis of mitochondria after building up EM

After formation of EM, bulk matrix extrusion from PN ceased, so PN got matured into nucleus (NU); while PC was not the case, in which new mitochondria were developed continuously even after the emergence of vacuoles (V) with internal vesicle (IV), multilamellar body (MLB), lipid droplet (LD), and small opaque vesicle (SOV), leading to the distortion of PMT (Fig.9). As shown in Fig.9A, a small mitochondrion was being developed at the PC edge; while a twisting dumbbell-shaped mitochondrion was nearly finished, one of its bulbous-end sequestering an internal body (ITB) was segregated, but another end was contiguous with PC (Fig.9B). Details of mitochondrion biogenesis were displayed during the assembly of giant mitochondria. As shown in Fig. 9C, a large unfinished 'L-shaped' mitochondrion was continuous with PC in the region around its corner point: the inner side envelope of its long arm and the corresponding portion of CHE, as well as the interior CR were nearly complete; while those of its short arm were just being synthesized. All these membranes were synthesized by merging the small dense-margined vesicles (DGV) developed from the segmented PMT (Fig.9C). Consequentially, mitochondria envelope

(ME) and the corresponding portion of CHE were consisted of two unit-membranes; while CR, like PT, ST and PMT, was delimited by a unit-membrane. Similarly, in another cell a bulky

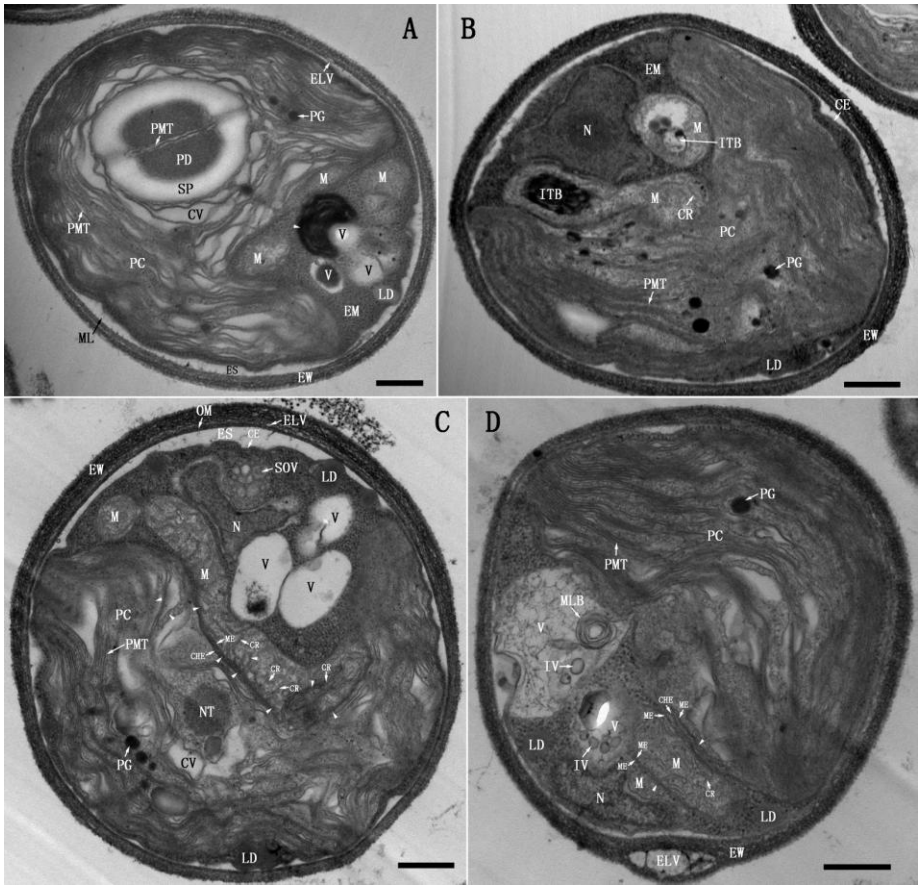

Figure 9. Biogenesis of mitochondria after building up EM. (**A)** After formation of EM, PN got matured into nucleus (N); while a small mitochondrion was being developed in PC in the presence of two mitochondria, three vacuoles (V), a lipid droplet (LD) and some electron-dense materials (arrowhead). (**B**) A twisting dumbbell-shaped mitochondrion was nearly finished, one of its bulbous-end containing an internal body (ITB) was segregated, but the other was contiguous with PC. Another mitochondrion within EM also sequestered an ITB. (**C**) A large 'L-shaped' mitochondrion was being assembled in the presence of three vacuoles and a cluster of small opaque vesicles (SOV), which was continuous with PC in the region around its corner point. The inner side mitochondrial envelope (ME) and the corresponding portion of CHE as well as CR were all synthesized by fusion of the dense-margined vesicles (DGV) (arrowhead) that were developed by segmentation of PMT. There was a large nucleoid-like structure (NT) in the venter side of PC. (**D**) After emergence of the large vacuoles with internal vesicle (IV) and multilamellar body (MLB), a bulky mitochondrion was being developed, which was connected with PC on the inner side but a small mitochondrion on the outer side. In the inner and outer interfaces, three and two pairs of contorted membranes were being synthesized respectively by merging DGV (arrowhead). In addition, several large ELV were embedded in EW. Scale bar, 0.5 μm.

mitochondrion was undergoing segregation, which was connected with PC on the inner side but a small mitochondrion on the outer side (Fig.9D). In the inner and outer interfaces, three and two pairs of contorted membranes were being synthesized respectively by fusion of DGV: among the three pairs of membranes, the outer and middle ones were the segments of ME and CHE

respectively, while the inner one was likely the envelope of the next mitochondrion that appeared to be in preparation; likewise the two pairs of membranes were the outer side and inner side ME of the bulky and small mitochondria respectively (Fig.9D).

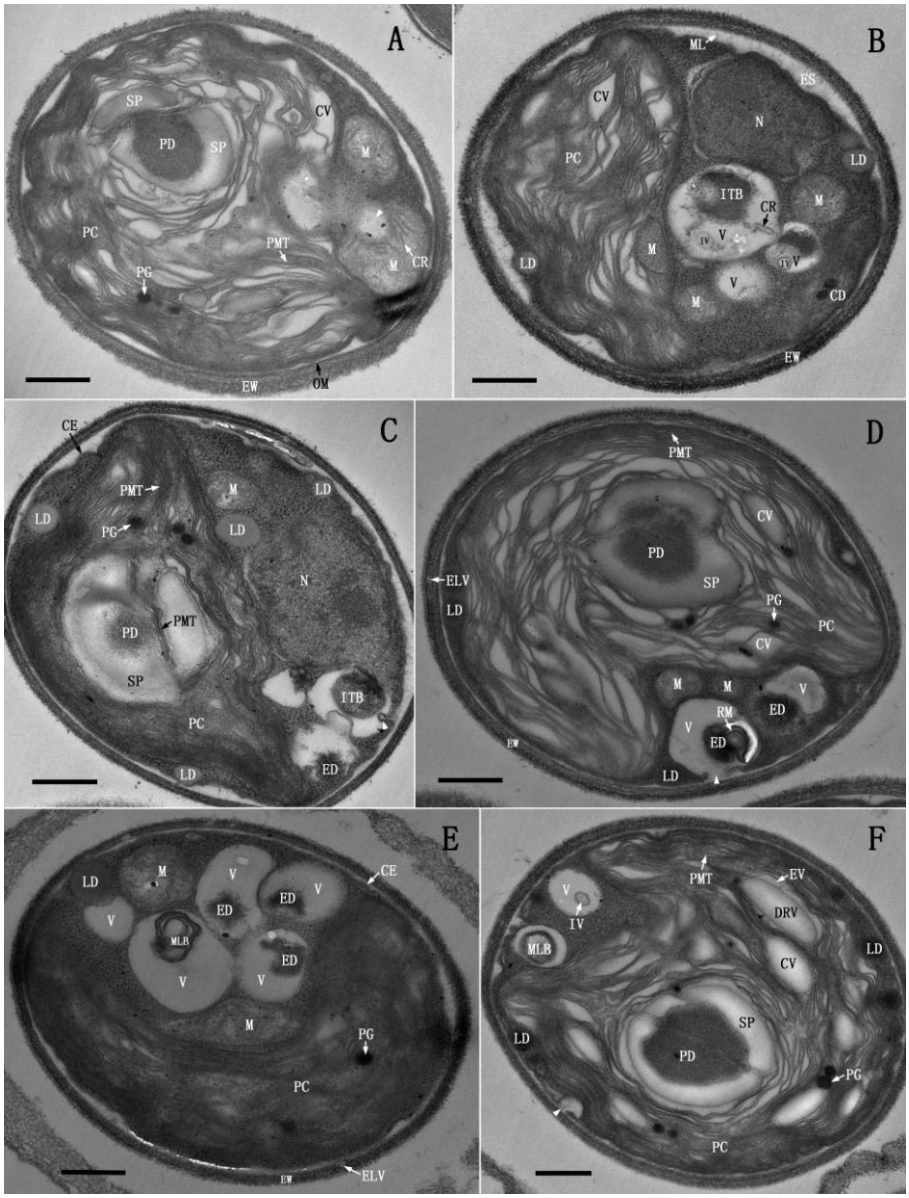

Figure 10. Biogenesis of vacuoles (**A**) The matrix of a mitochondrion was being degraded (arrowhead). (**B**) After matrix degradation, the mitochondrion turned into a vacuole containing ITB, IV and remnant CR or only electron-transparent matrix. Meanwhile, a new mitochondrion was being developed in PC, a LD was formed at CE and a piece of chloroplast debris (CD) emerged in EM. (**C**) ITB in two small mitochondria degraded into electron-dense debris (ED); while ITB in the large vacuole remained intact, the vacuolar membrane fused with CE and invaginated (arrowhead) (**D**) a small vacuole expelled ED into EM; while a large vacuole sequestered some residual membranes (RM), the membranes of which contacted and fused with CE, resulting in an opening (arrowhead). (**E**) A large vacuole contained MLB, while a small vacuole extruded a LD into EM. (**F**) Two vacuoles contained MLB and IV respectively. A small vacuole fused with CE, giving rise to an opening (arrowhead); and several cobblestone-shaped DRV emerged in EV. Scale bar, 0.5 μm.

2.6 Biogenesis of vacuoles and degradation of PMT-derived vesicles

2.6.1 Mitochondria turned into vacuoles after matrix-degradation

Following the emergence of new mitochondrion, the opaque matrix of previously formed mitochondrion began to degrade into transparent material (Fig. 10A), such that the mitochondria turned into double-membrane-bounded vacuoles (V), containing ITB, IV and remnant CR, or only electron-transparent matrix (Fig. 10B). In parallel with vacuole biogenesis, a new mitochondrion was assembled within PC, two LD were developed at CE and a piece of chloroplast debris (CD) emerged in EM (Fig.10B). Hereafter, most ITB decomposed into electron-dense debris (ED) (Fig.10C), which was subsequently expelled outside into EM (Fig. 10D); while some ITB themselves also contained small ITB, so after degradation of their contents, the residual membranes (Fig. 10D) collected into MLB (Paquet et al., 2013) (Fig, 10 EF).

2.6.2 Formation and degradation of PMT-derived vesicles and coalescence of vacuoles

After vacuoles came into being, some short PMT in PC curled and 'rolled up' into "vesicle within vesicle" like compound vesicles (CPV) (Fig.11 ABC), which were taken up by vacuoles directly as they got segregated from PC (Fig. 11C), or after they shed into EM (Fig.11AB). upon the internalized CPV released their contents for degradation, the remaining membranes stacked up into MLB (Fig. 11DEF). The vacuoles fused with each other by membrane protrusion. As shown in Fig. 11CD, a vacuole protruded into another one and fused at the contact sites, such that the membrane protrusion pinched off and became an IV (Fig.11E) or shed as MF (Fig. 11DF). When PC dwindled to a normal size, no more mitochondria and CPV were produced and all vacuoles coalesced into a large single one (Fig.11F). Hence, PC got matured into chloroplast (C) and as such PMT matured into eukaryotic thylakoids (T).

2.7 Vacuole mediated unconventional exocytosis and endocytosis

2.7.1 Vacuole-mediated unconventional exocytosis

Vacuoles came into contact and fuse with CE, and then the contacted membranes broke up into fragments resulting in large openings, from which a small quantity (Fig. 10DF; 12A) or a large amount of vacuolar content and SOV (Fig.12B) were expelled into ES. These expelled SOV were internalized from the neighboring SOV clusters (Fig.12B). Undoubtedly, the exocytotic materials contained proteins, which were not sorted through Golgi apparatus. Therefore, the vacuole-mediated exocytosis was an unconventional route of protein secretion (Nickel and Rabouille 2009; Ding et al., 2012; Zhang and Schekman, 2013).

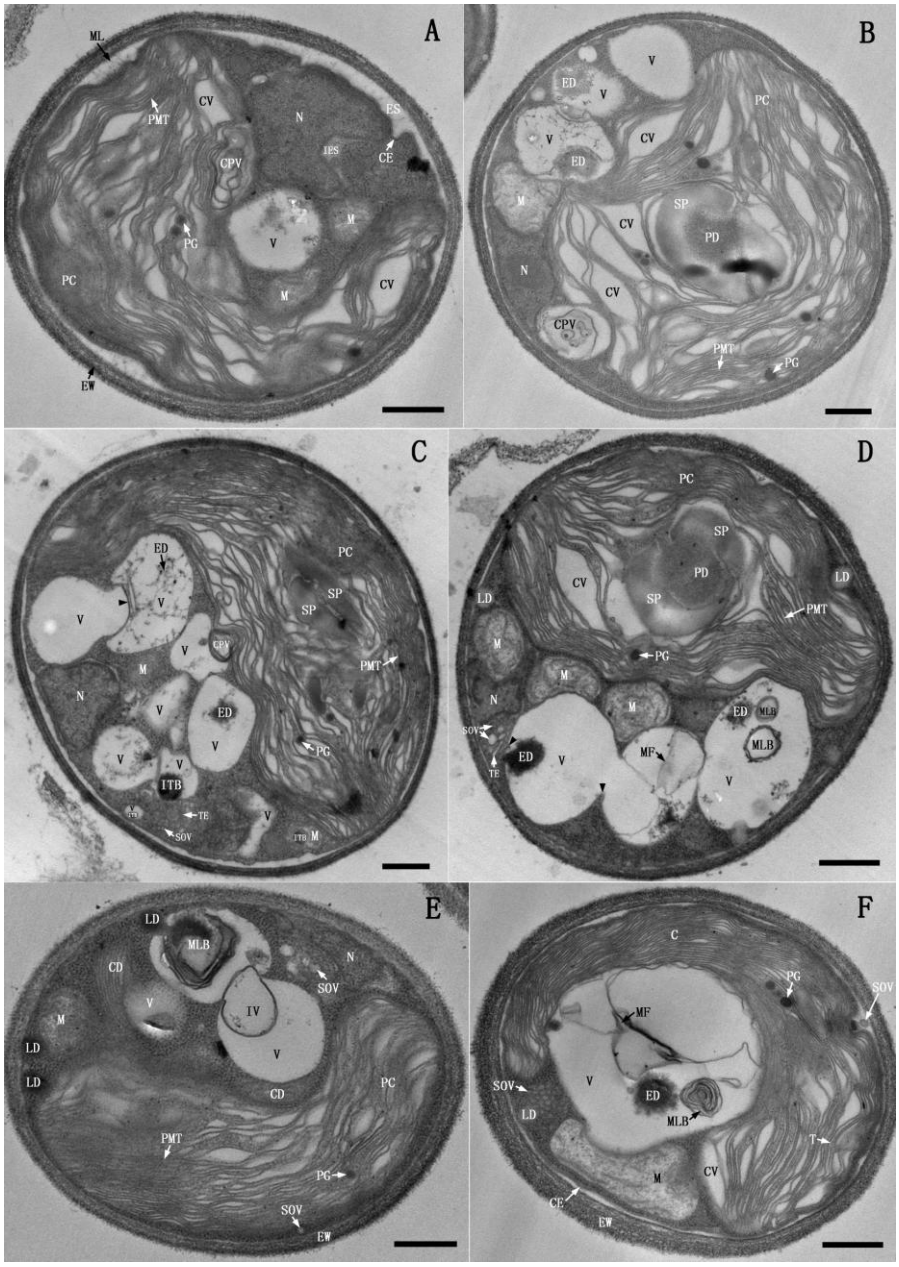

Figure 11. Formation and degradation of PMT-derived vesicles and coalescence of vacuoles. (**A**) A collection of short PMT 'rolled up' into "vesicle within vesicle" like compound vesicle (CPV) in PC margin. (**B**) A CPV was segregating from PC into EM. (**C**) A CPV was detaching from PC into a vacuole; while a large vacuole protruded into another one (arrowhead). (**D**) Membranes of the protruded vacuoles and the vacuole that contained membranous fragments (MF) fused at their contact site (arrowhead). (**E**) Two vacuoles were merging, in which a LD was extruded from MLB; while a conspicuous piece of CD presented in EM. (**F**) PC got matured in chloroplast (C); all vacuoles coalesced into a single vacuole containing ED, MF and MLB. Scale bar, 0.5 μm.

2.7.2 Vacuole-mediated unconventional endocytosis

The double-membranes of vacuole merged with CE at two distant sites and then invaginated, resulting in a large invaginated space (IVS), entrapping some electron-dense fibrils (EF) and globular particles (GP); while CE between the two merged sites disrupted and coiled into

membranous structures (Fig.12C). Upon IVS reaching certain size, the membrane invagination pinched off into the vacuole lumen and became a large IV, whose content was degraded in situ or discharged into the vacuole lumen (Fig.12D). In the same way, the nascent vacuole also mediated small episode of endocytosis (Fig.10C). Evidently, the vacuole-mediated endocytosis was an unconventional endocytic route and distinct form the conventional endocytosis.

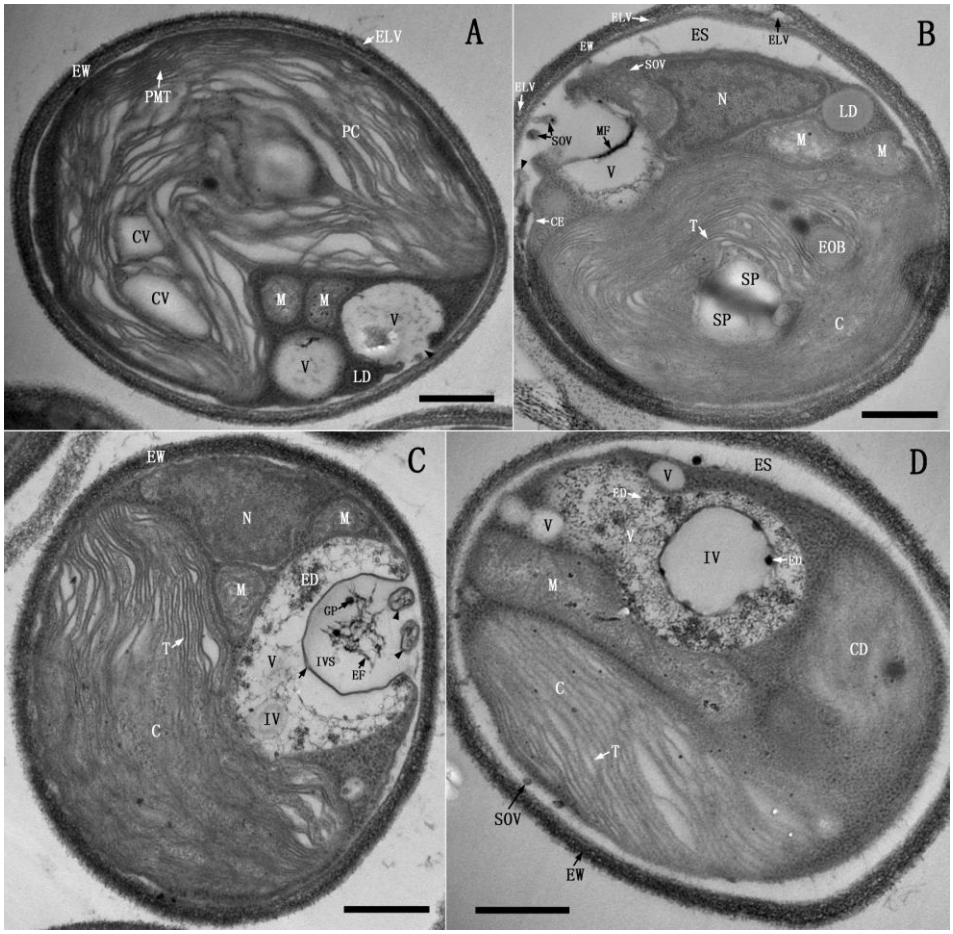

Figure 12. Vacuole mediated unconventional exocytosis and endocytosis. (**A)** An opening was formed at the contact site of the vacuolar membranes and CE (arrowhead), from which the vacuolar content was released. (**B**) The contacted vacuolar membranes and CE broke up into fragments (arrowhead)，resulting in a wide opening, from which the soluble contents and SOV were expelled outside into ES. (**C**) The vacuolar membranes merged with the CE at two distant sites and then invaginated, resulting in a large invaginated space (IVS) entrapping some electron-dense fibrils (FB) and globular particles (GP); while CE between the two merged sites disrupted and coiled into membranous structures (arrowhead). It was clear that the invaginated vacuolar membranes consisted of two unit membranes (arrow). (**D**) A vacuole contained a large IV, which was in contact with a sausage-shaped mitochondrion and close to a CD. Scale bar, 0.5 μm.

2.8 Structure and reproduction of the TDX16-derived eukaryotic cell

After bulk exocytosis and endocytosis, the large vacuoles disappeared, while the distorted thylakoids in the chloroplast straightened with narrowed luminal spaces (Fig.13ABC). As a result,

the prokaryotic TDX16 cell (Fig.1-2) developed eventually into a stable eukaryotic cell with unique structure (Fig.13ABC). The TDX16-derived eukaryotic cell (TDX16-DE cell) was surrounded by an OM-containing EW, an ES of variable widths and a double-membraned CE, containing a characteristic "e-shaped" chloroplast, a nucleus with OE and NE, usually two

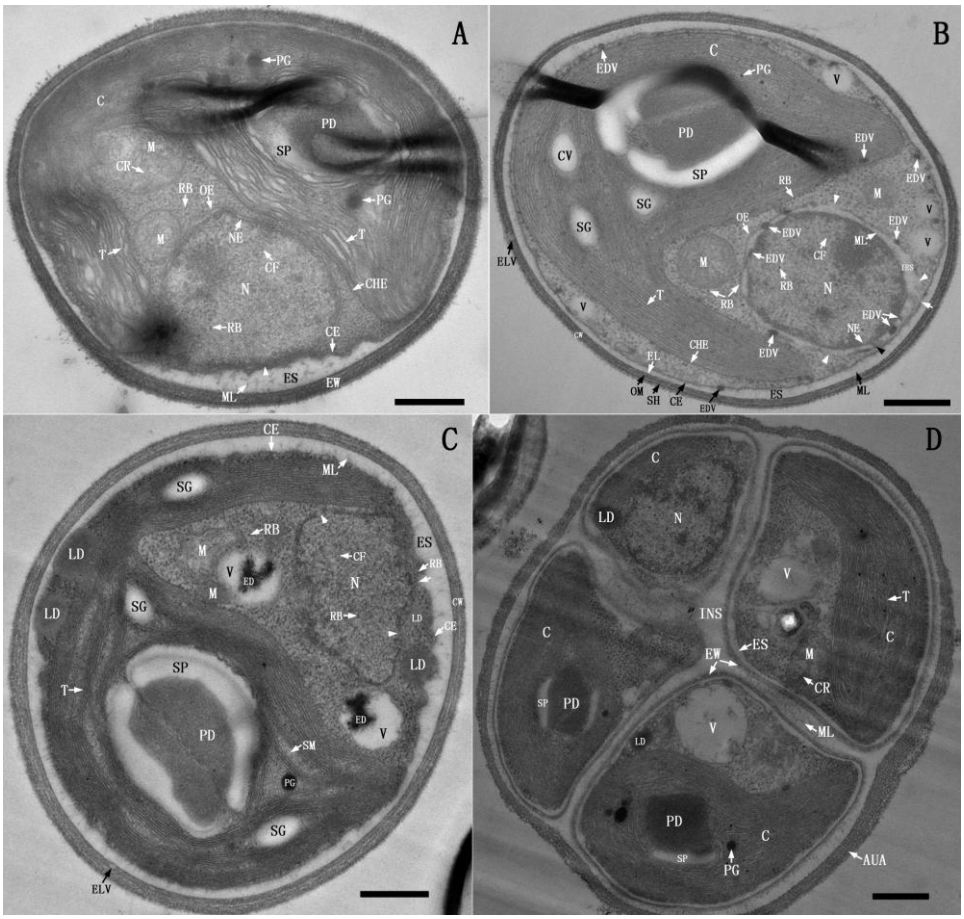

Figure 13. Structure and reproduction of TDX16-derived eukaryotic cell. (**A**) A TDX16-derived eukaryotic cell (TDX16-DE cell) contained an 'e'-shaped chloroplast (C), a nucleus (N) and two mitochondria. The nucleus contained CF and some RB, whose OE and NE contacted and appressed to CE at the opening of chloroplast cavity (arrowhead). (**B**) Electron-dense vesicles (EDV) budded form NE (black arrowhead) into IES, and then fused with and re-budded from OE, ultimately reached the inner side of CHE and the two sides of CE. There were several openings at OE (white arrowhead), and one opening at the contact site of OE and CE (arrow). (**C**) OE and NE contacted intimately, on which large openings (arrowhead) were formed, and amazingly a fusion pore or conduit was formed at the contact site of NE, OE and CE (arrow). (**D**) Four developing autospores in an autosporangium (AUA) were segregated from each other by the wide interspace (INS). Scale bar, 0.5 μm.

mitochondria and frequently two or more small double-membrane-bounded vacuoles, but no endoplasmic reticulum, Golgi apparatus and peroxisomes (Fig.13ABC). Hence, OE, NE and CE served dual or multiple functions; while OM and ES consistently played similar roles as they did before organelle biogenesis (Fig. 1-6), though their composition and content apparently changed. The large nucleus with no visible pores on OE and NE still contained a few RB (Fig.13ABC).

When OE and NE became widely separated, some electron-dense vesicles (EDV) budded form NE into IES, and then fused with and re-budded from OE, ultimately migrated to the inner leaflet of CHE as well as the inner and outer leaflets of CE (Fig.13B), which delivered probably nucleus-synthesized proteins for maintaining the corresponding envelope membranes. If so, the transportation of nucleus-synthesized proteins into ES with NE-derived vesicles was another way of unconventional exocytosis. During this process OE disrupted locally resulting in several openings, and more importantly, an opening was also formed at the contact site of OE and CE. Such that the proteins synthesized in EM could be sorted through OE openings into IES and then secreted via the opening on CE into ES (Fig. 13B). By contrast, when OE and NE came into contact, they fused at several sites and thus gave rise to openings, allowing nucleocytoplasmic transport (Fig.13C). Amazingly, a fusion pore was formed at the contact site of NE, OE and CE (Fig.13C), enabling the direct communication between nucleus and ES.

TDX16-DE cell multiplied via autosporulation. As shown in Fig.13D, four autospores within an autosporangium (AUG) were segregated from each other by the wide interspace, more or less similar in arrangement to TDX16 (endospores) in the sporangium (Fig.1).

2.9 Photosynthetic pigments of TDX16 and TDX16-DE cell

In vivo absorption spectra (Fig.14A) showed that apart from the absorption maxima of chlorophyll a (Chl a) at 440 and 680 nm, TDX16 displayed a prominent peak at 630nm, corresponding to phycocyanin (Lemasson et al., 1973); while TDX16-DE cell exhibited a conspicuous shoulder peak of chlorophyll b (Chl b) at 653 nm (Govindjee and Rabinowitch, 1960), and a merged peak of carotenoids around 485 nm. Consistent with these results, fluorescence emission spectroscopy indicated that the water soluble pigment extract of TDX16 (Fig. 14E) and lipid soluble pigment extract of TDX16-DE (Fig. 14F) displayed an emission peak of phycocyanin at 646 nm (Gantt et al., 1979) and an emission peak of Chl b at 658 nm (Thorne et al., 1977) respectively, but no emission peak was detected in the water soluble pigment extract of TDX16-DE (Fig. 14E) and lipid soluble pigment extract of TDX16 (Fig. 14F). Furthermore, phycocyanin isolated from TDX16 had an absorption peak at 617nm (Fig. 14B), nearly the same as C–phycocyanin (Gantt et al., 1979); Chl b and lutein separating from TDX16-DE cell displayed absorption maxima at 456 and 645 nm (Fig. 14C), 420, 446 and 475nm (Fig. 14D) respectively, identical to those isolated from plants (Lichtenthaler, 1987).

2.10 16S rRNA sequences of TDX16 and TDX16-DE cell

16S rRNA of TDX16 (GenBank KJ599678.2) and TDX16-DE chloroplast (GenBank KJ612008.1)

shared a low identity of 83%, but showed high similarities of 98% and 99% to that of *Chroococcidiopsis thermalis* (GenBank NR102464.1) and those of the chloroplasts of *Auxenochlorella protothecoides* (GenBank AY553213.1) and *Chlorella vulgaris* (GenBank AB001684.1) respectively.

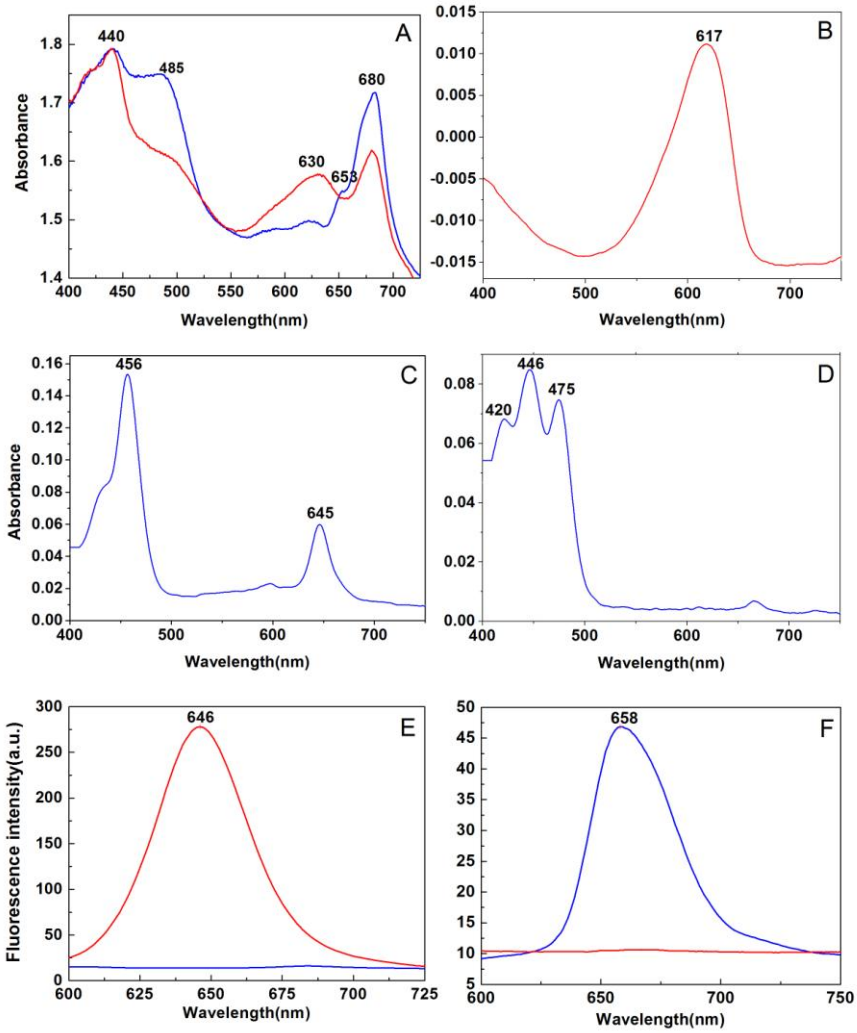

Figure 14. Absorption and fluorescence emission spectra. (**A**) In vivo absorption spectra of TDX16 (red) and TDX16-DE cell (blue). Absorption spectra of phycocyanin (**B**), chlorophyll b (**C**) and lutein (**D**). Fluorescence emission spectra of water soluble pigment extracts (**E**) and lipid soluble pigment extracts (**F**) of TDX16 (red) and TDX16-DE cell (blue).

2.11 Genome sequence of TDX16

TDX16 genome was 15,333,193 bp in size with an average of GC content of 55.2 % containing 15,894 genes (CDS 15,756; RNA 138). This Whole Genome Shotgun project has been deposited at DDBJ/ENA/GenBank under the accession NDGV00000000. The version described in this paper is version NDGV01000000.

3. Discussion

3.1 The reason for organelle biogenesis in TDX16

The consistent results of cell structure (Fig.1-2), pigmentation (Fig.14) and 16S rRNA gene sequence indicated that TDX16 is a phycocyanin-containing cyanobacterium resembling *C. thermalis*. However the genome size, gene number and GC content of TDX16 (GenBank NDGV00000000) are 2.4, 2.8 and 1.2 times those of *C. thermalis* (6,315,792 bp, 5593 genes and 44.4% GC) (GenBank CP003597.1) respectively. Since TDX16 is an endosymbiotic cyanobacterium released from the senescent/necrotic cell of green alga *H. pluvialis* (Dong et al., 2011), these results demonstrated that TDX16 had acquired at least 9,017,401bp DNAs with 10301 genes from its host. Accordingly, the reason for organelle biogenesis in TDX16 was the expression of hybrid genome formed by hybridizing the acquired eukaryotic DNAs with TDX16's prokaryotic ones, the process of which was indicated by the changes of cell structures:

(1) the obtained DNAs were retained most likely in the replicable HGBs, which contained DNA-like materials, situated in NU and remained a constant size in different cells (Fig.1);

(2) when compartmentalization commenced, the obtained DNAs were released gradually from HGB into the NU (Fig. 3), most of which kept inactive because the initially formed PT were cyanobacterial ones, owing apparently to the expression of TDX16's own genes that were inhibited within the host cell (Fig.4);

(3) the total DNAs in the solubilized ICP were fragmented, intermingled and hybridized into new genome (Fig.5 and 6), which was subsequently partitioned into NS (major portion) and NIC (minor portion);

(4) the dismantling of PL and absence of PCB in the transitional PT-derived ST (Fig. 6) indicated the initial expression of new hybrid genome. And then PC and PN were formed by sequestering the DNAs in NIC and NS, respectively (Fig.7). Thereafter, DNAs in PN became nuclear genome; DNAs in PC became compound genome, from which the mitochondrial genome was assembled, while the remaining DNAs were organized into chloroplast genome (Fig. 8-11). So, it was not surprising that mitochondrial and chloroplast genomes shared similar features, and chloroplast genome retained some mitochondrion-related genes. The disappearance of PC (Fig. 14), PL (Fig. 7) and TDX16 16S rRNA, but appearance of chlorophyll b, lutein (Fig.14) and 16S rRNA in TDX16-DE chloroplast indicated that DNA hybridization involved the loss of some prokaryotic genes and the synthesis new genes. The detail molecular mechanism is currently unclear, and awaits further elucidation.

3.2 Some long-standing questions in cell biology become clear

Organelle biogenesis in TDX16 is an intricate and subtle process, during which some long-standing questions in cell biology become clear:

(1) OG and PG are the precursors of thylakoids in cyanobacteria and chloroplasts respectively;

(2) mitochondrial cristae, like thylakoids, are not formed by invagination of the inner membrane;

(3) MLBs are developed from mitochondrion and chloroplast;

(4)vacuoles and nucleus-derived vesicles mediate unconventional exocytosis;

(5) there is an OM in EW, and thus ES is a membrane-surrounded compartment;

(6) LDs are produced predominantly at CE but marginally at CHE.

3.3 Implications of organelle biogenesis in TDX16

Organelle biogenesis in cyanobacterium TDX16 (prokaryote) resulted in its transition into a new green alga TDX16-DE (eukaryote). It is reasonable that prokaryote-to-eukaryote transition is not confined to TDX16, and other prokaryotes (cyanobacteria and bacteria), are also capable of such transitions under the similar conditions. Hence, organelle biogenesis in TDX16 has profound implications in cell biology, particularly cancer cell biology, and evolutionary biology.

Cancer cells are thought to be transformed from the normal cells, however, recent studies reveal that the small nascent primary cancer cells (PCCs) for cancer initiation (Walen, 2002, 2004; Sundaram et al., 2004; Leikam et al., 2015; Zhang et al., 2016) and secondary cancer cells (SCCs) for cancer progression (Buikis et al., 1999; Erenpreisa et al., 2000; Sundaram et al., 2004; Puig et al., 2008; Ianzini et al., 2009; Weihua et al., 2011; Zhang et al., 2013; Niu et al., 2016, 2017; Zhang et al., 2017) are formed in and but not transformed from the senescent normal cells and cancer cells, respectively. These small nascent PCCs/SCCs are very small, undifferentiated (Todaro and Green, 1963; Woodworth et al., 1988; Buikis et al., 1999; Romanov et al., 2001; Niu et al., 2017) and absent of organelles resembling bacteria, which mature into eukaryotic PCCs/FCCs after being released from the ruptured senescent normal/cancer cells. Nevertheless, the cellular mechanisms of how the small nascent PCCs/SCCs are formed, and how the organelles are developed in PCCs/SCCs are unclear. In the light of TDX16-to-TDX16-DE transition, it seems most likely that PCCs/SCCs arise from bacteria: the intracellular bacteria take up the senescent normal/cancer cells' DNAs and retain them in the replicable HGB-like single-membrane-delimited "micronuclei" (Pontén et al., 1963) and thus become small nascent organelle-less PCCs/SCCs; after liberation, the small nascent PCCs/SCCs mature into eukaryotic PCCs/SCCs by hybridizing the acquired DNAs with their own ones and expressing the hybrid genomes, during which organelles are formed de novo in a way akin to organelle biogenesis in TDX16.

In evolutionary biology, it is hypothesized that an archaebacterium in a eubacterial host became a nucleus, whereby the host turned into an eukaryote; and then a bacterium and a

cyanobacterium entered this eukaryote and became a mitochondrion and a chloroplast respectively. Different from this hypothesis, organelle biogenesis in TDX16 suggests that (1) organelles are not derived from but are formed in the endosymbiotic prokaryotes that had acquired hosts' DNAs; (2) organelle biogenesis in prokaryotes is not only once in ancient time but continues after the emergences of eukaryote ancestor. So, part or all of the single-celled eukaryotes are derived from prokaryotes, whose evolutionary history can not be inferred or reconstructed by gene or genome-based phylogenetic analyses. (3) hybridization of prokaryotic and eukaryotic DNAs and partition of the hybrid ones during organelle biogenesis in prokaryotes give the false impression of prokaryote to eukaryote "horizontal (lateral) gene transfer" and "interorganellar gene transfer" in eukaryotes.

4. Materials and methods

4.1 Strain and culture

Pure culture of TDX16 in BG-11 medium (Stanier et al., 1971) was maintained under low light intensity of 12 μmol photons m^{-2} s^{-1}, at 25 ℃ in the illumination incubator (Dong et al., 2011). For experiment, TDX16 was inoculated into sterilized 250-ml Erlenmeyer flasks containing 100 ml BG-11 medium and incubated under high light intensity of 60 μmol photons m^{-2} s^{-1}, at 25 ℃.

4.2 Microscopy preparations and observations

Cells were fixed with 2.5% glutaraldehyde and 1% osmium tetroxide, followed by dehydration with ascending concentrations of ethanol, and post staining with 3% uranyl acetate and lead citrate. The samples were examined with a JEM1010 electron microscope (JEOL, Japan).

4.3 Pigment analyses

4.3.1 In vivo absorption spectra

Cell suspensions were scanned with Ultraviolet-Visible Spectrophotometer Cary 300 (Agilent, USA), the spectra were normalized to give an equal absorbance of Chl a at 440 nm.

4.3.2 Fluorescence emission spectra

Water soluble pigments were extracted with 0.75M K-phosphate buffer (pH= 6.8). Lipid soluble pigments were extracted with pure acetone and diluted 50-fold into ethanol. Both extracts were analyzed directly on Fluorescence Spectrophotometer F-4500 (Hitachi, Japan) at room temperature with excitations of 580 and 478 nm respectively.

4.3.3 Pigment separation and identification

Chl b was separated by thin-layer chromatography according to the method described by Lichtenthaler (Lichtenthaler, 1987). phycocyanin was extracted and purified following the procedures described by Adams (Adams et al., 1979). All pigments were analyzed with Ultraviolet-Visible Spectrophotometer Cary 300 (Agilent, USA), and identified by spectroscopic matching with the published data.

4.4 16S rRNA sequence

DNA samples were prepared according to the method described previously (Garcia-Pichel et al., 1998). 16S rRNAs were amplified using the primers 8-27f (AGAGTTTGATCCTGGCTCAG) and 1504-1486r (CTTGTTACGACTTCACCCC) (Moore et al., 1998). Fragments were cloned into the pMD18-T vector and amplified using M13 forward and reverse universal primers. The PCR products were digested with restriction enzymes BamH1/SalI, and sequenced on ABI 3730 DNA analyzer (PerkinElmer Biosystems, USA).

4.5 Genome sequence of TDX16

TDX16 cells were harvested by centrifugation at 3000 rpm for 10 min, and washed twice with 5M NaCl solution and sterile water alternately, with the pelleted cells being frozen in liquid nitrogen and then grinded with sterile glass beads (0.5 mm diameter).The slurry was transferred into 5ml centrifuge tube with TE buffer (1mM EDTA, 10 mM Tris-HCl, pH=8.0), supplemented with 1.0 ml lysozyme solution (20 mg/ml) and incubated at 37℃for 60 min, then added CTAB (Cetyltrimethyl ammonium bromide) solution (10% CTAB, 0.7 M NaCl) and heated to 65℃ for 30 min in a waterbath. After centrifugation (12000 rpm, 10min), the supernatant was extracted with one volume of phenol-chloroform-isoamyl alcohol (25:24:1, V/V), and DNA was precipitated overnight at −20 ℃ after the addition of 2/3 volume of cold isopropanol and 1/10 volume of 3M sodium acetate, dried and resuspended in TE buffer. The extracted DNA was first subjected to quality assay and then sheared ultrasonically into fragments, with their overhangs being converted into blunt ends applying T4 DNA polymerase, Klenow Fragment and T4 Polynucleotide Kinase. Subsequently, adapters were ligated to the 3' ends of DNA fragments that were introduced with ‘A’ bases. The obtained fragments were purified via gel-electrophoresis and PCR-amplified for preparing the sequencing library of DNA clusters. Paired-end sequencing was carried out on an IIlumina HiSeq 4000 platform, yeilding1.132 Mb raw data. After removal of the low quality reads, 1.009 Mb clean data was assembled with SOAPdenovo.

References

Adams, S.M., Kao, O.W and Berns, D.S (1979) Psychrophile C-Phycocyanin. Plant Physiol. 64: 525–527.

Allen, M. M (1984) Cyanobacterial cell inclusions. Annu. Rev. Microbiol. 38:1-25.

Alvarez, H. M., Mayer, F., Fabritius, D., and Steinbüchel, A (1996) Formation of intracytoplasmic lipid inclusions by *Rhodococcus opacus* strain PD630. Arch. Microbiol. 165:377–386

Aseeva, E., Ossenbuhl, F., Sippel, C., et al. (2007) Vipp1 is required for basic thylakoid membrane formation but not for the assembly of thylakoid protein complexes. Plant Physiol. Biochem. 45: 119–128

Aubert, S., Gout, E., Bligny, R., Marty-Mazars, D., Barrieu, F., Alabouvette, J., Marty, F. and Douce, R (1996) Ultrastructural and biochemical characterization of autophagy in higher plant cells subjected to carbon deprivation: control by the supply of mitochondria with respiratory substrates. J. Cell Biol. 133: 1251–1263

Austin, J.R., Frost, E., Vidi, P.A., Kessler, F., and Staehelin, L.A (2006) Plastoglobules are lipoprotein subcompartments of the chloroplast that are permanently coupled to thylakoid membranes and contain biosynthetic enzymes. Plant Cell 18: 1693–1703

Bennoun P (1982) Evidence for a respiratory chain in the chloroplast. Proc. Natl. Acad. Sci. USA 79: 4352–4356

Bevis, B. J., Hammond, A. T., Reinke, C. A., and Glick, B. S (2002) De novo formation of transitional ER sites and Golgi structures in Pichia pastoris. Nature Cell Biol. 4, 750–756

Billi, D., Friedmann, E. I., Hofer, K.G., Caiola, M.G and Friedmann, R.O(2000) Ionizing-radiation resistance in the desiccation-tolerant cyanobacterium *Chroococcidiopsis*. Appl. Environ. Microbiol. 66:1489–1492

Bréhélin, C., Kessler, F and van Wijk, K. J (2007) Plastoglobules: versatile lipoprotein particles in plastids. Trends plant sci. 12 (6):260-266

Buikis, I., Harju, L and Freivalds, T (1999) Origin of microcells in human sarcoma cell line HT1080. Anal Cell Pathol. 18: 73-85.

Bullejahn, G. S and Sherman, L. A (1986) Identification of a Carotenoid-Binding Protein in the Cytoplasmic Membrane from the Heterotrophic Cyanobacterium *Synechocystis* sp. Strain PCC6714. J. Bacteriol. 167: 396-399

Caiola, M. G., Friedmann, R. C and Friedmann, E.I (1993) Cytology of long-term desiccation in the desert cyanobacterium *Chroococcidiopsis* (Chroococcales). Phycologia 32: 315-322.

Davidi, L., Levin, Y., Ben-Dor, S and Pick, U (2015) Proteome analysis of cytoplasmatic and plastidic b-carotene lipid droplets in *Dunaliella bardawil*. Plant Physiol. 167: 60–79

De Toledo, G. A., Fernandez-Chacon, R and Fernandez, J. M. (1993). Release of secretory products during transient vesicle fusion. Nature 363: 554–558.

Ding, Y., Wang, J., Wang, J.Q., Stierhof, Y. D., Robinson, D. G., and Jiang, L. W (2012) Unconventional protein secretion. Trends Plant Sci. 17:606-615.

Dong, Q. L., Li, Z.W., Xing, X.Y., Chen, B (2011) Discovery of an endophytic cyanobacterium in *Haematococcus pluvialis*. J. Hebei Univ.Technol. 40: 1-5

Egan, A.J., Cleverley, R.M., Peters, K., Lewis, R.J., and Vollmer, W. (2016) Regulation of bacterial cell wall growth. FEBS J. 284: 851-867

Eltsov, M., and Zuber, B (2006) Transmission electron microscopy of the bacterial nucleoid. J. Struct. Biol. 156:246–54

Erenpreisa, J., Cragg, M., Fringes, B., Sharakhov, I and Illidge, T (2000) Release of mitotic descendents by giant cells from irradiated burkitt's lymphoma cell line. Cell Biol Int. 24: 635-648

Fan, J., Andre, C., and Xu, C (2011) A chloroplast pathway for the de novo biosynthesis of triacylglycerol in *Chlamydomonas reinhardtii*. FEBS Lett. 585:1985-1991.

Fan, L., Li, R., Pan, J., Ding, Z., and Lin, J (2015) Endocytosis and its regulation in plants. Trends Plant Sci. 20: 388-397

Forbes, D. J., Kirschner, M.W., Newport, J.W (1983) Spontaneous formation of nucleus-like structures around bacteriophage DNA microinjected into Xenopus eggs. Cell 34:13–23

Gantt, E., and Conti, S. F (1969) Ultrastructure of blue-green algae. J. Bacteriol. 97: 1486-1493

Gantt, E., Lipschultz, C. A., Grabowski, J., and Zimmerman, B .K. (1979) Phycobilisomes from blue-green and red algae: isolation criteria and dissociation characteristics. Plant Physiol. 63: 615–620.

Gao, H., and Xu, X (2009) Depletion of Vipp1 in *Synechocystis* sp. PCC 6803 affects photosynthetic activity before the loss of thylakoid membranes. FEMS Microbiol. Lett. 292: 63–70.

Garcia-Pichel, F., Nübel, U., and Muyzer, G (1998) The phylogeny of unicellular, extremely halotolerant cyanobacteria. Arch. Microbiol. 169, 469–482.

Gibbs, S.P (1962) The ultrastructure of the pyrenoids of green algae. J. Ultra. Res. 7: 262-272.

Govindjee, and Rabinowitch, E (1960) Two forms of chlorophyll a in vivo with distinct photochemical functions. Science 132: 355-356.

Hay, E. D., and J. P. Revel (1963) The fine structure of the DNP component of the nucleus. J. Cell Biol. 16:29-51

Harding, C., Heuser, J., and Stahl, P (1983) Receptor-mediated endocytosis of transferrin and

recycling of the transferrin receptor in rat reticulocytes. J. Cell Biol. 97:329–339.

Hoh, B., Hinz, G., Jeong, B. K., and Robinson, D.G (1995) Protein storage vacuoles form de novo during pea cotyledon development. J. Cell Sci. 108, 299-310

Hoiczyk, E., and Hansel, A (2000) Cyanobacterial cell walls: news from an unusual prokaryotic envelope. J. Bacteriol. 182: 1191-1199

Ianzini, F., Kosmacek, E.A., Nelson, E.S., Napoli, E., Erenpreisa, J., Kalejs, M and Mackey, M.A (2009) Activation of meiosis-specific genes is associated with depolyploidization of human tumor cells following radiation-induced mitotic catastrophe. Cancer Res. 69: 2296-2304.

Keren, N., Liberton, M., and Pakrasi, H. B (2005) Photochemical competence of assembled photosystem II core complex in cyanobacterial plasma membrane. J. Biol. Chem. 280: 6548–6553

Kim, P. K., Mullen, R. T., Schumann, U., and Lippincott-Schwartz, J (2006) The origin and maintenance of mammalian peroxisomes involves a de novo PEX16-dependent pathway from the ER. J. Cell Biol. 173: 521–532

Lang, N. J (1968) The fine structure of blue-green algae. Ann. Rev. Microbiol. 22: 15-46.

Leikam, C., Hufnagel, A.L., Otto, C., Murphy, D.J., Muhling, B., Kneitz, S., Nanda, I., Schmid, M., Wagner, T.U., Haferkamp, S., Brocker, E.B., Schartl, M and Meierjohann, S (2015) In vitro evidence for senescent multinucleated melanocytes as a source for tumor-initiating cells. Cell Death Dis. 6:e1711. doi: 10.1038/cddis.2015.71

Lemasson. C., Marsac, N. T., and Cohen-Bazire, G (1973) Role of allophycocyanin as a light-harvesting pigment in cyanobacteria. Proc. Nat. Acad. Sci. USA 70: 3130-3133.

Li, H. M., Kaneko, Y., and Keegstra, K (1994) Molecular cloning of a chloroplastic protein associated with both the envelope and thylakoid membranes. Plant Mol. Biol. 25: 619–632.

Lippincott-Schwartz, J and Zaal, K. J (2000) Cell cycle maintenance and biogenesis of the Golgi complex. Histochem. Cell Biol. 114: 93–103

Liberton, M., Berg, R. H., Heuser, J., Roth, R., and Pakrasi, H. B (2006) Ultrastructure of the membrane systems in the unicellular cyanobacterium *Synechocystis* sp strain PCC 6803. Protoplasma 227: 129–138

Lichtenthaler, H. K(1987) Chlorophylls and carotenoids: pigments of photosynthetic biomembranes. Methods Enzymol. 148, 350–382.

Lichtenthaler, H. K (2013) Plastoglobuli, thylakoids, chloroplast structure and development of plastids. In: Biswal B, Krupinska K, Biswal UC (eds) Plastid development in leaves during growth and senescence advances in photosynthesis and respiration. Springer, Berlin, pp

337–361.

Lohka, M. J and Y. Masui. 1984. Roles of and cytoplasmic particles in nuclear envelope assemble and sperm pronuclear formation in cell-free preparations from amphibian eggs. J. Cell Biol. 98:1222-1230.

Lowe, M and Barr, F. A (2007) Inheritance and biogenesis of organelles in the secretory pathway. Nat. Rev. Mol. Cell. Biol. 8:429–439.

Marty, F (1999) Plant vacuoles. Plant Cell 11:587-600

McMahon, H. T., and Boucrot, E (2011) Molecular mechanism and physiological functions of clathrin-mediated endocytosis. Nat. Rev. Mol. Cell Biol. 12: 517–533

Meindl, U., Lancelle, S., and Hepler, P. K (1992) Vesicle production and fusion during lobe formation in Micrasterias visualized by high-pressure freeze fixation. Protoplasma 170:104--114

Moore, L. R., Rocap, G., and Chisholm, S. W (1998). Physiology and molecular phylogeny of coexisting *Prochlorococcus* ecotypes. Nature 393: 464–467.

Mullineaux, C. W (2014) Co-existence of photosynthetic and respiratory activities in cyanobacterial thylakoid membranes. Biochim. Biophys. Acta 1837: 503–511

Nickel, W., and Rabouille, C (2009) Mechanisms of regulated unconventional protein secretion. Nat. Rev. Mol. Cell Biol. 10:234-255

Niu, N., Zhang, J., Zhang, N., Mercado-Uribe, I, Tao, F., Han, Z et al.(2016) Linking genomic reorganization to tumor initiation via the giant cell cycle. Oncogenesis 5, e281; doi:10.1038/oncsis. 75

Niu, N., Mercado-Uribe, I., Liu, J (2017) Dedifferentiation into blastomere-like cancer stem cells via formation of polyploid giant cancer cells. Oncogene. 36: 4887–900.

Osborn, M. J., Gander, J. E., Parisi, E., and Carson, J (1972) Mechanism of assembly of outer membrane of *Salmonella typhimurium*: Isolation and characterization of cytoplasmic and outer membrane. J. Biol. Chem. 247:3962-3972.

Pan, B.T., Teng, K., Wu, C., Adam, M., and Johnstone, R.M (1985) Electron microscopic evidence for externalization of the transferrin receptor in vesicular form in sheep reticulocytes. J. Cell Biol. 101:942-948

Paquet, V.E., Lessire, R., Domergue, F., Fouillen, L., Filion, G., Sedighi, A., Charette, S.J (2013) Lipid composition of multilamellar bodies secreted by *Dictyostelium discoideum* reveals their Amoebal origin. Eukaryotic Cell 12: 1326–1334.

Peramuna, A., and Summers, M. L (2014) Composition and occurrence of lipid droplets in the cyanobacterium *Nostoc punctiforme*. Arch. Microbiol. 196: 881–890

Peschek, G.A., Hinterstoisser, B., Wastyn, M., Kuntner, O., Plneau, E., Missblchler, A., and Lang, J (1989) Chlorophyll precursors in the plasma membrane of a cyanobacterium *Anacystis nidulans*. J. Biol. Chem. 264: 11827-11832.

Pontén, J., Jensen, F and Koprowski, H (1963) Morphological and virological investigation of human tissue cultures transformed with SV40. J. Cell. and Comp. Physiol. 61: 145-163.

Puig, P.E., Guilly, M.N., Bouchot, A., Droin, N., Cathelin, D., Bouyer, F et al. (2008) Tumor cells can escape DNA-damaging cisplatin through DNA endoreduplication and reversible polyploidy. Cell Biol Int 32: 1031–1043.

Ren, L., Mellander, L., Keighron, J., Cans, A. S., Kurczy, M., Svir, I., Oleinick, A., Amatore, C., Ewing, A. G (2016) The evidence for open and closed exocytosis as the primary release mechanism. Q. Rev. Biophys. 49, e12.

Rexroth, S., Mullineaux, C. W., Ellinger, D., Sendtko, E., Rögner, M., and Koenig, F (2011) The plasma membrane of the cyanobacterium *Gloeobacter violaceus* contains segregated bioenergetic domains. Plant Cell 23: 2379–2390.

Rippka, R., Waterbury, J., and Cohen-Bazire, G (1974) A cyanobacterium which lacks thylakoids. Arch. Microbiol. 100: 419–436.

Romanov, S. R., Kozakiewics, B. K., Hoist, C. R., Stampfei, M. R., Haupt, L. M and Tlsty, T. D (2001) Normal human mammary epithelial cells spontaneously escape senescence and acquire genomic changes. Nature 409:633-637

Rothman, J. E., and Wieland, F. T (1996) Protein sorting by transport vesicles. Science 272: 227–234.

Saftig P., and Klumperman, J (2009) Lysosome biogenesis and lysosomal membrane proteins: trafficking meets function. Nat. Rev. Mol. Cell Biol. 10: 623–635

Samuels, A. L., Giddings, T. H., and Staehelin, L. A (1995) Cytokinesis in tobacco BY-2 and root tip cells: a new model of cell plate formation in higher plants. J. Cell Biol. 130: 1345–1357

Schatz, G., and Dobberstein, B (1996) Common principles of protein translocation across membranes. Science 271:1519–1526.

Schekman, R., and Orci, L (1996) Coat proteins and vesicle budding. Science 271: 1526–1533.

Simon, R. D (1971) Cyanophycin granules form the blue-green alga *Anabaena cylindrica*: a reserve material consisting of copolymers of aspartic acid and arginine. Proc. Natl. Acad. Sci. USA 68:265–267.

South, S. T and Gould, S. J (1999) Peroxisome Synthesis in the Absence of Preexisting Peroxisomes. J. Cell Biol. 144: 255–266

Stanier, R. Y., Kunisawa, R., Mandel, M., and Cohen-Bazire, G. (1971). Purification and properties

of unicellular blue-green algae (Order Chroococcales). Bacteriol. Rev. 35: 171-205.

Sugiura, A., Mattie, S., Prudent, J., and McBride, H. M (2017) Newly born peroxisomes are a hybrid of mitochondrial and ER-derived pre-peroxisomes. Nature 542: 251–254

Sundaram, M., Guerrnsey, D.L., Rajaraman, M.M., Rajaraman, R.R (2004) Neosis: a novel type of cell division in cancer. Cancer Biol Therap 3:207-218.

Théry, C., Zitvogel, L., and Amigorena, S (2002) Exosomes: composition, biogenesis and function. Nat. Rev. Immunol. 2: 569-579

Thorne, S.W., Newcomb, E.H., and Osmond, C.B (1977) Identification of chlorophyll b in extracts of prokaryotic algae by fluorescence spectroscopy. Proc. Natl. Acad. Sci. USA 74: 575–578.

Todaro, G. J and Green, H (1963) Quantitative studies of the growth of mouse embryo cells in culture and their development into established lines. J. Cell Biol. 17: 299-313.

van de Meene, A. M., Hohmann-Marriott, M. F., Vermaas, W. F., Roberson, R. W (2006) The three-dimensional structure of the cyanobacterium *Synechocystis* sp. PCC 6803. Arch. Microbiol. 184: 259–270

van der Zand, A., Gent, J., Braakman, I., and Tabak, H. F (2012) Biochemically distinct vesicles from the endoplasmic reticulum fuse to form peroxisomes. Cell 149: 397–409.

Vidi, P., Kanwischer, M., Baginsky, S., Austin, J. R., Csucs, G., Dörmann, P., Kessler, F., and Bréhélin, C (2006) Tocopherol cyclase (VTE1) localization and vitamin E accumulation in chloroplast plastoglobule lipoprotein particles. J. Biol. Chem. 281: 11225–11234

Viotti, C., et al. (2013) The endoplasmic reticulum is the main membrane source for biogenesis of the lytic vacuole in *Arabidopsis*. Plant Cell 25:3434–3449.

Walen, K.H (2002) The origin of transformed cells: studies of spontaneous and induced in cell cultures from marsupials, a snail and human amniocytes. Cancer Genet Cytogenet 133:45-54.

Walen, K.H (2004) Spontaneous cell transformation: karyoplasts derived from multinucleated cells produce new cell growth in senescent human epithelial cell cultures. In Vitro Cell Dev Biol Anim. 40:150-158.

Weihua, Z., Lin, Q., Ramoth, A.J., Fan, D and Fidler, I.J (2011) Formation of solid tumors by a single multinucleated cancer cell. Cancer 117: 4092–4099

Westphal, S., Heins, L., Soll, J., and Vothknecht, U. C (2001) Vipp1 deletion mutant of *Synechocystis*: a connection between bacterial phage shock and thylakoid biogenesis? Proc. Natl. Acad. Sci. USA 98: 4243–4248.

Woodcock, C.L., Frado, L.L and Rattner, J.B (1984) The higher order structure of chromatin:

evidence for a helical ribbon arrangement. J. Cell Biol. 99, 42–52.

Woodworth, C. D., Bowden, P. E., Doninger, J., Pirisi, L., Barnes, W., Lancaster,W. D and DiPaolo, J.A (1988) Characterization of normal human exocervical epithelial cells immortalized in vitro by papillomavirus types 16 and 18 DNA. Cancer Res. 48:4620-4628.

Yeates, T. O., Kerfeld, C. A., Heinhorst, S., Cannon, G. C., and Shively, J. M (2008) Protein-based organelles in bacteria: carboxysomes and related microcompartments. Nat. Rev. Microbiol. 6: 681–691

Ytterberg, A. J., Peltier, J., and van Wijk, K. J (2006) Protein profiling of plastoglobules in chloroplasts and chromoplasts. A surprising site for differential accumulation of metabolic enzymes. Plant Physiol. 140: 984–997

Zak, E., Norling, B., Maitra, R., Huang, F., Andersson, B., and Pakrasi, H. B (2001) The initial steps of biogenesis of cyanobacterial photosystems occur in plasma membranes. Proc. Natl. Acad. Sci. USA 98:13443–13448

Zhang, M., and Schekman, R (2013) Cell biology. Unconventional secretion, unconventional solutions. Science 340:559-561.

Zhang, S., Shen, S., Li, Z., Golbeck, J. H., and Bryant, D.A (2014) Vipp1 is essential for biogenesis of Photosystem I but not thylakoid membranes in *Synechococcus* sp. PCC7002. J. Biol. Chem. 289: 15904–15914.

Zhang, S., Mercado-Uribe, I., Liu, J (2013) Generation of erythroid cells from fibroblasts and cancer cells in vitro and in vivo. Cancer Lett 333: 205–212.

Zhang, S., Mercado-Uribe, I., Sood, A., Bast, R.C., Liu, J (2016) Coevolution of neoplastic epithelial cells and multilineage stroma via polyploid giant cells during immortalization and transformation of mullerian epithelial cells. Genes Cancer 7: 60–72.

Zhang, D., Yang, X.Y., Yang, Z. D. et al (2017) Daughter cells and erythroid cells budding from pgccs and their clinicopathological significances in colorectal cancer. J Cancer 8:469–478.

Acknowledgements

This work was supported by the Natural Science Foundation of Hebei Province (B2008000029).

Author contributions

Q.L.D and X.Y.X. performed the experiment and wrote the manuscript with the participation of Y.H in partial electron microscopic observation and 16S rRNA sequencing, X.L.W and S. Z in pigment analyses.

List of abbreviations

AUG	Autosporangium
C	Chloroplast
CD	Chloroplast debris
CE	Cytoplasmic envelope
CF	Chromatin fibers
CG	Cyanophycin granules
CHE	Chloroplast envelope
CLM	Cloudlike materials
CM	Cytoplasmic membrane
CPV	Compound vesicles
CR	Cristae
CV	Combined vesicles
CW	Cell wall
CX	Carboxysomes
DF	DNA Fibers
DGV	Dense-margined vesicles
DLF	DNA-like fibrils
DMF	Double-layered membrane fragment
DMS	Double-layered membrane segment
DMV	Double-membraned vesicles
DRV	Dilated ring-shaped vesicles
DSV	Dense vesicle
DT	DNA threads
DV	Dotted vesicles
ED	Electron-dense debris
EDV	Electron-dense vesicles
EF	Electron-dense fibrils
EG	Electron-dense granules
EIS	Empty Inner space
EL	Electron-dense layer
ELM	Electron-translucent materials
ELV	Electron-translucent vesicles
EM	Eukaryotic cytoplasm
EOB	Electron-opaque bodies
EOP	Electron-opaque particles
EOM	Electron-opaque materials
EOV	Electron-opaque vesicles
EP	Electron-dense particles
EPM	Electron-transparent materials
ER	Endoplasmic reticulum
ES	Extracytoplasmic space
EV	Electron-transparent vesicle
EW	Eukaryotic cell wall
FM	Fibrillary materials
GA	Golgi apparatus
GP	Globular particles
HGB	Heterogenous globular bodies
IB	Intranuclear body
ICE	Intracytoplasmic envelope
ICP	Inner cytoplasm
IES	Inter envelope space
IIM	Inner intracytoplasmic membrane
IIS	Inner intracytoplasmic space
INS	Interspace
IS	Intracytoplasmic space
ITB	Internal body
IV	Internal vesicle
IVS	Invaginated space
LD	Lipid droplet
LDB	Less electron-dense bodies
LDM	Less electron-dense materials
LM	Limiting membrane
M	Mitochondrion
ME	Mitochondrial envelope
MF	Membrane fragments
ML	Microfibrils
MLB	Multilamellar body
MR	Margin residues
MS	Membrane segments
MT	Membranous elements
MV	Microvesicles
N	Nucleus
NE	Nuclear envelope
NIC	New inner cytoplasm
NIS	New inner intracytoplasmic space
NS	New intracytoplasmic space
NT	Nucleoid-like structure
NU	Nucleoid
NX	New intracytoplasmic matrix
OCP	Outer cytoplasm
OE	Outer nuclear envelope
OG	Osmiophilic granules
OIM	Outer intracytoplasmic membrane
OIS	Outer intracytoplasmic space

OPV	Opaque-periphery vesicle	SA	Sporangium
OM	Outer membrane	SG	Starch granules
OV	Oblong vesicles	SH	Sheath
P	Peptidoglycan layer	SMV	Smaller vesicles
PB	Polyphosphate bodies	SM	Stroma
PC	Primitive chloroplast	SOV	Small opaque vesicle
PCB	Phycobilisomes	SP	Starch plate
PD	Pyrenoids	ST	Secondary thylakoids
PG	Plastoglobuli	SV	Small vesicles
PL	Peptidoglycan-like layer	T	Thylakoids
PMT	Primitive thylakoids	TE	Tubules
PN	Primitive nucleus	TL	Thylakoid-like structure
PNE	Primitive nuclear envelope	TMF	Two-layered membrane fragment
PO	Pores	TMV	Thick margin vesicle
PT	Primary thylakoids	TV	Tiny vesicles
RB	Ribosomes	V	Vacuole
RM	Residual membranes	VB	Vesicle-containing body
RV	Ring-shaped vesicles		